INFLUENCE OF CARBON ALLOTROPIC FORMS ON OUTPUT VOLTAGE AND CURRENT IN TRIBOELECTRIC NANOGENERATOR

YOLTAWAN SINSANONG
UTCHAWADEE PHARINO

A SPECIAL PROJECT SUBMITTED IN PARTIAL FULFILLMENT OF
THE REQUIREMENT FOR
THE DEGREE OF BACHERLOR OF SCIENCE (INDUSTRIAL CHEMISTRY)
DEPARTMENT OF CHEMISTRY FACULTY OF SCIENCE
KING MONGKUT'S INSTITUTE OF TECHNOLOGY LADKRABANG
ACADEMIC YEAR 2018

Title	Influence of Carbon Allotropic Forms on Output Voltage and Current in Triboelectric Nanogenerator.
Students	Miss. Yoltawan Sinsanong Student ID 58050533
	Miss. Utchawadee Pharino Student ID 58050576
Degree	Bachelor of Science in Industrial Chemistry
Department	Chemistry
Faculty	Science
University	King Mongkut's Institute of Technology Ladkrabang (KMITL)
Academic	Year 2018
Advisor	Assoc. Prof. Dr. Naratip Vittayakorn

Abstract

The triboelectric nanogenerators (TENGs) is a new kind of energy technology that can harvest ambient mechanical energy and convert it into electricity for powering small electronic devices. In this report, we demonstrated the simple templating method to fabricate elastically deformed Polydimethylsiloxane (PDMS) sponge. The porous structure of the PDMS sponges is controllable and exhibit similar shape with the used templates particles. Our results showed that Young's modulus and tensile strength of a PDMS sponge are dependent on its uniformity of pores. The Young's modulus of PDMS sponge is reduced of a factor ~ 4 -7 time by the different pore structure and PDMS sponge using salt particles as templates exhibited the softest sponge. The results also show that the salted template PDMS sponge performs the highest output voltage and current. The results also show that the PDMS sponge using the salt template delivers the highest output voltage and current. Besides, the graphitic carbon nitride (g-C3N4) and Graphite fluoride composite with PDMS sponge were successfully fabricated by the salt-templating method. The composite of g-C3N4/PDMS sponge exhibited ultrahydrophobic behavior and large Young's modulus. The dielectric constant of the composite increased with increasing the g-C_3N_4 concentration. However, the relationship between electrical output performance with the level of g-C_3N_4 did not seem in this work. The similar behavior was also observed in the Graphite fluoride/ PDMS sponge composite.

Keywords: nanogenerator, polydimethylsiloxane, sponge, templating, triboelectric

ACKNOWELDGEMENT

First, I would like to thank my thesis advisor, Assoc. Prof. Dr. Narathip Vittayakorn, for the opportunity to study in the bachelor's degree of Science in academic year 2018. He gave us everything for guidance and supporting in our thesis for 1 year. We have developed a greater potential, especially skills of thinking and reasoning. Also, we profoundly appreciative that he gave us for advice in addition to the work and pulled us up from distress when we had barriers.

I would like to thank Asst. Prof. Dr. Panpailin Seeharaj and Dr. Chaval Sriwong for as thesis committee, suggestion, reviewed this thesis, and some useful comments.

Next, I would like to thank Dr. Thitirat Charoonsook, Dr.Saichon Sriphan and all members of Advance materials research laboratory.

Finally, we would like to thank you for our family and friends to always beside and help we until finish this work done.

Yoltawan Sinsanong
Utchawadee Pharino

CONTENTS

LIST OF TABLES

Table **Page**

LIST OF FIGURES

Figure **Page**

ABBREVIATIONS AND SYMBOLS

Abbreviations/Symbols	Explain
BS	Brown sugar
CAM	Citric Acid Monohydrate
CBS	Cube brown sugar
CNTs	Carbon nanotubes
CWS	Cube white sugar
FOTS	Perfluorrooctyltrichlorosilane
FT-IR	Fourier Transform Infrared spectroscopy
g.C_3N_4	Graphitic carbon nitride
GO	Graphene oxide
MSG	Monosodium glutamate
NaCl	Sodium chloride
PDMS	Polydimethylsiloxane
PLA	Polylactic acid
PMMA	Polymethyl methacrylate
PNC	Porous nanocomposite
PS	Polystyrene
PTFE	Poly-(tetrafluoroethylene)
PVDF	Polyvinylidene fluoride
SDS	Sodium dodecyl sulfate
SEM	Scanning Electron Microscope
TENG	Triboelectric nanogenerator
V	Voltage
WS	White sugar
XRD	X-ray diffraction

CHATER 1
INTRODUCTION

1.1 Motivation

In the past two decades, a dramatic trend in the progress of portable and wearable electronics for applications in health care, communication, and environmental monitoring. These devices require only power in microwatt (μW) to milliwatt (mW) level. However, they commonly rely on batteries causes the demand for batteries increases annually. Consequently, the quantity of waste batteries is also quickly increasing. Waste batteries contain large amounts of heavy metals and harmful materials, which damage to the ecological environment and human health.[1] Therefore, an innovation for harvesting energy from our environment have become important. Moreover, the stability of the energy sources is also realized because it guarantees long-term operation of devices. Then, there is considerable interest in mechanical energy as a power source due to its ubiquity and availability.[2] Triboelectric nanogenerators (TENGs) have attracted attention as an alternative to harvesting energy due to its high efficiency, cost effectiveness and environmental friendliness. Since the first demonstration by Wang in 2012, TENGs have been demonstrated bring about to the significant increasing of the instantaneous power density up to several tens of mW/cm^2. Therefore, TENG has become an important innovation in energy harvesting.[3, 4]

In principle, electrical energy is generated by the coupling between triboelectrification and electrostatic induction, Triboelectric effect is a type of charges transferred on the surfaces of two dissimilar materials after contact, and these charges induce electric potential between the conductive electrodes when they are separated. This induced potential drives the flow of mobile charges between the two electrodes.[5] There are numerous ways to improve the output of TENGs, the first way is to design a suitable device for energy harvesting from the energy source. The second way is the selection of the suitable materials. In addition, the surface and inner structure of materials can be modified to improve the output performance.[6]

Polydimethylsiloxane (PDMS) has been commonly used in TENGs due to its good triboelectric properties, superior flexibility and stretching, and non-toxicity. TENGs working based on dynamic motion so, the durability of material is important. Therefore, many researchers fabricated PDMS to porous structure in various ways, such as 3D-printing, phase separation, templating, *etc*. Compared with non-porous structure, they have more potential to maintain their shape under mechanical deformations.[7 - 12]

Besides pure PDMS, many researches improved its properties by embedding various materials, such as piezoelectric materials (i.e., Polyvinylidene fluoride (PVDF),

Barium titanate ($BaTiO_3$)[13]), conductive materials (i.e., Carbon nanotubes (CNTs)[14] [15] [16], Graphene [17], Liquid metal[18], etc.) and so on. For this improvement not only enhance the surface electrification but also the intrinsic of materials can be improved.

We fabricated the TENG base on contact separation mode to harvest energy from foot pressure. The device consisted of two layers. One layer, based on a hybrid of carbon allotropes including graphite fluoride and graphitic carbon nitride ($g\text{-}C_3N_4$) as dispersed phase in PDMS phase, was fabricated to be porous by templating. For the other layers, Al was used to investigate the output voltage and current in TENG.

1.2. Objectives of this work

1) To study the morphology, mechanical and electrical properties of sponge PDMS that was fabricated by different type of particles as a template.
2) To investigate the influence of carbon allotropic forms on mechanical and electrical properties of composite PDMS sponge.

1.3 Scope of this work

1) Fabrication of the PDMS sponge by using sacrificial templates, including cube white sugar, cube brown sugar, white sugar crystals, brown sugar crystals, salt crystals, and monosodium glutamate crystals
2) Fabrication of the composite PDMS sponge by mixing several carbon allotropic forms including 1,3,5,10 wt% of $g\text{-}C_3N_4$ and 10,20,40,60 wt% graphite fluoride in PDMS by using salt crystals templates
3) Characterization of PDMS and composite PDMS sponge by using scanning electron microscope (SEM), X–ray diffraction (XRD), Fourier-transform infrared spectroscopy (FTIR), contact angle measurement and compression testing
4) Measurement the electrical property of the TENG including the open circuit voltage and short circuit current
5) Measurement the dielectric property of the TENG including dielectric constant and dielectric loss.

1.4 Expected benefits

1) The fabrication of PDMS sponge by using sacrificial templates obtaining uniform characteristics.
2) The fabrication of composite PDMS sponge by mixing several carbon allotropes and polymer piezoelectric.
3) To improvement the output performance of the TENG

CHAPTER 2
LITERATURE REVIEW

Triboelectric nanogenerator (TENGs) has many advantages, including high efficiency, high power density and low cost. Therefore, TENGs become an important innovation in energy harvesting technologies. In this chapter we describe the fundamentals of the fabrication and development for TENGs.

2.1 Fundamental of Triboelectric nanogenerator

Triboelectric nanogenerator is a device that can covert mechanical energy into electricity. Movement of the electric dipole in one material relative to another (different) material generates an electric current, this effect was call triboelectrification, for this effect we can meet in every day including electrostatic.

Triboelectricity is a charge changing effect by contact pair of materials. After certain materials were contact with different material become electrically charge on the surface believe that formed a chemical bonding between some area of two surfaces. The electrons are moving and transfer charge to other materials for balance the potential between two surface become neutral electrochemical potential. When two surfaces are separated, some the bonded atom hold the electron, and some give or release. This mechanism made charge changing on the surfaces. Wang defined mode of Triboelectric in four way [19].

2.1.1 Vertical contact-separation mode

This mode is a simplest structure design of TENGs (Figure. 1a), two dielectric materials were contact and separated in the vertical and each material are deposited the electrode on the top and bottom surfaces of the structure. A physical contact between two dielectric films creates oppositely charged surfaces. Once the two surfaces are separated by a small gap by applying an external force, a potential drop is created. If the two electrodes are electrically connected by a load, free electrons in one electrode had flow to the other electrode to build an opposite potential in order to oppose the electrostatic field. Once the gap is closed, the triboelectric charge-created potential disappears, and the electrons flow back [19].

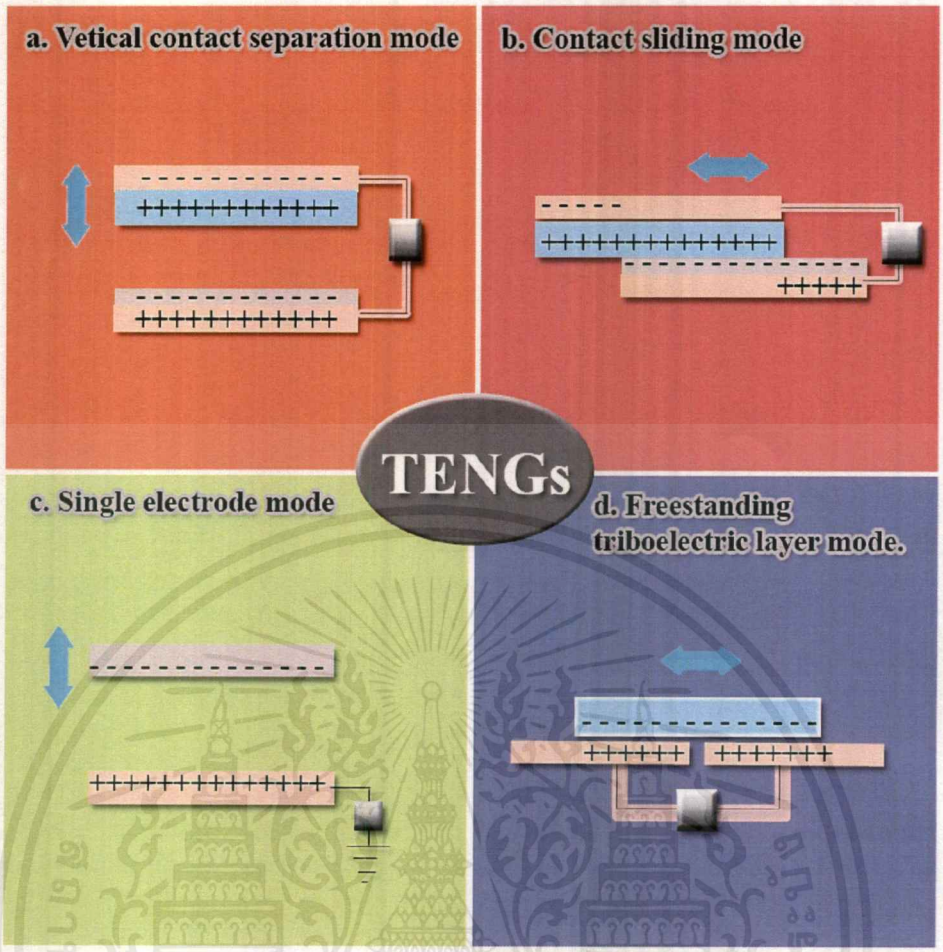

Figure 2.1 The four fundamental modes of triboelectric nanogenerators: (a) vertical contact separation mode, (b) contact-sliding mode, (c) single-electrode mode, and (d) freestanding triboelectric-layer mode [19].

2.1.2. Contact sliding mode

This structure is like the vertical contact-separation mode. When two dielectric materials were contact, sliding one relative to the other and parallel to the surface also creates triboelectric charges on the two surfaces (Figure. 1b). A lateral polarization is thus introduced along the sliding direction, which drives the electrons on the top and bottom electrodes to flow in order to fully balance the field created by the triboelectric charges. A periodic sliding apart and closing generates an electrical output. The sliding can be a planar motion or a rotation [20].

2.1.3. Single-electrode mode

The two modes introduced in Sections 1 and 2 have two electrodes interconnected by a load. Such TENGs can freely move so that they can work in mobile systems. This mode can use in some cases that the TENGs part cannot be electrically connected to the load, because it is mobile, such as a human walking on a floor. In order to harvest energy from this, a single electrode TENG can be formed, in which the

electrode on the bottom part of the TENG is grounded (Figure. 1c). If the size of the TENG is finite, a movement of the top object relative to the bottom one changes the local electrical field distribution, so that the electrons are exchange between the bottom electrode and the ground to create a potential difference.

2.1.4. Freestanding triboelectric-layer mode

On the surface of a moving object is charged due to it always contact with other materials or objects until the charge density are maximum. The structure (Figure. 1d) fabricated by deposited the pair of electrodes under dielectric layer, size of electrodes and the gap between two electrodes are equal as size of moving object. The approach and/or departure from electrodes create an asymmetric charge distribution in the object then become the electron flow to balance the different potential distribution. This mode can apply to harvesting the energy in many ways, for example, our shoes walking on the floor polar. Some case the moving object not directly touch to the top of dielectric layer of the electrodes such as in rotation mode [21].

2.2 Triboelectric materials

Triboelectric series is a table are separate the materials which has a tendency easy to gain (negative) or loose (positive) the electron capability of a material follow the table below. After selected the triboelectric nanogenerator mode we can increase the potential of the work by choosing the pair of triboelectric materials from this table because of the triboelectrification present a good effect when two materials are having a high different potential between two materials.

Table 2.1 Triboelectric series [22]

Polyformaldehyde 1.3-1.4	Polyester (Dacron) polyisobutylene
Ethylcellulose	Polyurethane flexiblesponge
Polyamide16 Polyamide6-6	Polyethylene Terephthalate
Melanime formol	Polyvinyl butyral
Wood, knitted	Polycholobutadiene
Silk, woven	Natural rubber
Aluminum	Polyacrilonitile
Paper	Acrylonitile-vinly chloride
Cotton, woven	Polybisphenol carbonate
Steel	Polycholoether
Wood	Polyvinlylidine chloride (Saran)
Nickle, copper	Polyethylene

Positive

Sulfur	Polypropylene
Brass, Silver	Polyimide (Kapton)
Acetate, rayon	Polyvinyl chloride (PVC)
Polymethyl methacrylate (Lucite)	**Polydimethylsiloxane (PDMS)**
Polyvinyl alcohol	Polytetrafluoroethylene (Teflon)

Negative

Accordingly, many work about triboelectric nanogenerator use the Polydimethyl siloxane (PDMS) to be based structure because their properties, Flexible, stretch ability, easy to fabricated in micro or nanopattern, suitable for human use, environmental friendly (non-toxic) and its deep negative section in the triboelectric series that can describe PDMS has a tendency to gaining (negative) the electron capability. Metal is the popular one of triboelectric material because of it tends to lose (positive) the electron capability, easy to be found in daily life (commercial) and low cost.

In our work we selected to fabricate the triboelectric nanogenerator PDMS based in vertical contact separation mode because it has easy structure, easy fabricated, suitable for harvesting energy from human activities and environmentally friendly.

In addition, we have many ways to increasing the output performance of TENGs such as, Modifying the surface morphology or inner structure [23], engineering structure of PDMS such as fabrication a sponge PDMS [24] and add the dispersed phase to PDMS for fabrication a composite [25] that we will mention in the next section.

2.3 Composite materials

Composites are the combinations of materials differing in composition or form on a macroscale. The constituents retain their identities in the composite, that is they do not dissolve or otherwise merge completely into each other although they act in concert. Normally, the components can be physically identified and exhibit an interface between one another. A composite material is made by combining two or more materials, often ones that have very different properties. The two materials work together to give the composite unique properties. Most composites are made of two materials, one is the main matrix or binder and other matrix or dispersed phase is sometimes to as reinforcement and/or improve some properties to the materials [26].

Many researches modified PDMS to from composites with various kinds of materials including conductive materials, semiconductors, dielectrics, piezoelectric materials to enhance the electrical output. The allotropes of carbon are the one group of materials that have been extensively used, for example graphene, carbon nanotube, graphite fluoride, graphitic carbon nitride and poly-vinylidene fluoride, one of the

reasons is they have a good electrical conductivity from benzene rings on graphene structure, some also have the asymmetric structures or functional groups estimated that can make some interesting output results.

The example research at below is demonstrate some appropriate properties of the allotropes of carbon that enhance the electrical properties and increasing the electrical output.

The report names "Synergism of graphitic-carbon nitride and electrospinning on the physico-chemical characteristics and piezoelectric properties of flexible poly(vinylidene fluoride) based nanogenerator [27]", they demonstrate the increasing output voltage and output current by adding the Graphitic carbon nitride ($g\text{-}C_3N_4$) nanosheets in the piezoelectric performance of electrospun poly(vinylidene fluoride)/graphitic carbon nitride (PVDF/$g\text{-}C_3N_4$) nanocomposite fibers (PGN-X).

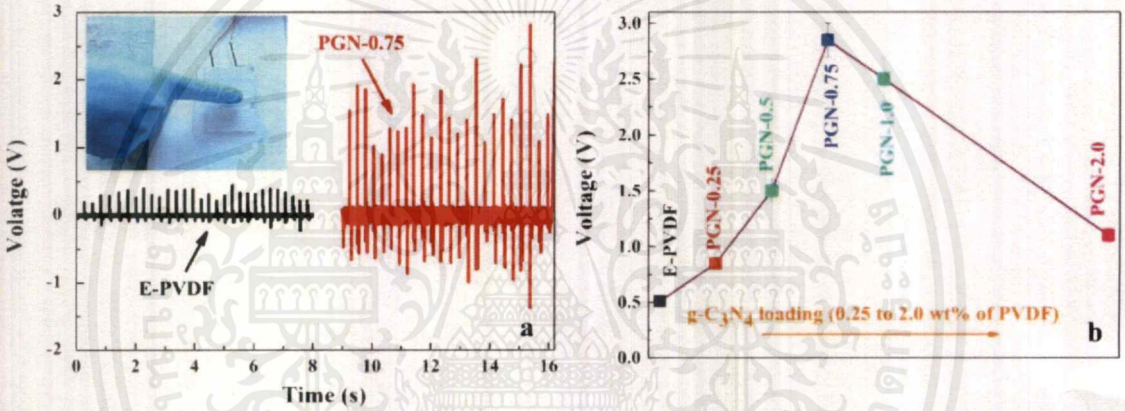

Figure 2.2 Piezoelectric performance of (a) E-PVDF, and b PGN-X for different loading of $g\text{-}C_3N_4$ under one finger tapping mode [27]

Next example research is about the piezoelectric performance of E-PVDF and PGN-X based nanogenerator. Electrospun nanofiber mat was sandwiched between two interdigitated copper electrodes (3.0 × 2.0 × 0.01 cm). The electrodes were then covered with a flexible non-conducting sheet made of poly(vinyl chloride). In Figure.2a they show the output voltage generated upon one finger tapping on E-PVDF and PGN-0.75 based nanogenerator. For E-PVDF maximum voltage output was 0.6 V while, for PGN-0.75 it was 2.6 V. Also, the piezoelectric voltage output improved with an increase in g-C3N4content. It is important to note that the voltage output increased up to 0.75 wt% of $g\text{-}C_3N_4$ loading, thereafter a decline was observed in the output (Figure.2.2 b).

In the next work they present a power-generating sensor array in a flexible and stretchable form. The proposed device is composed of resistive strain sensors, capacitive tactile sensors, and a triboelectric energy harvester in a single platform. The device is implemented in a woven textile structure by using proposed functional threads include, the inner surface of the tube is coated with 1H, 1H, 2H, 2H-

perfluorrooctyltrichlorosilane (FOTS) to have a high output power form the electron affinity of fluoride atom during the energy-harvesting operation of the device by changing the triboelectric property of the surface [28].

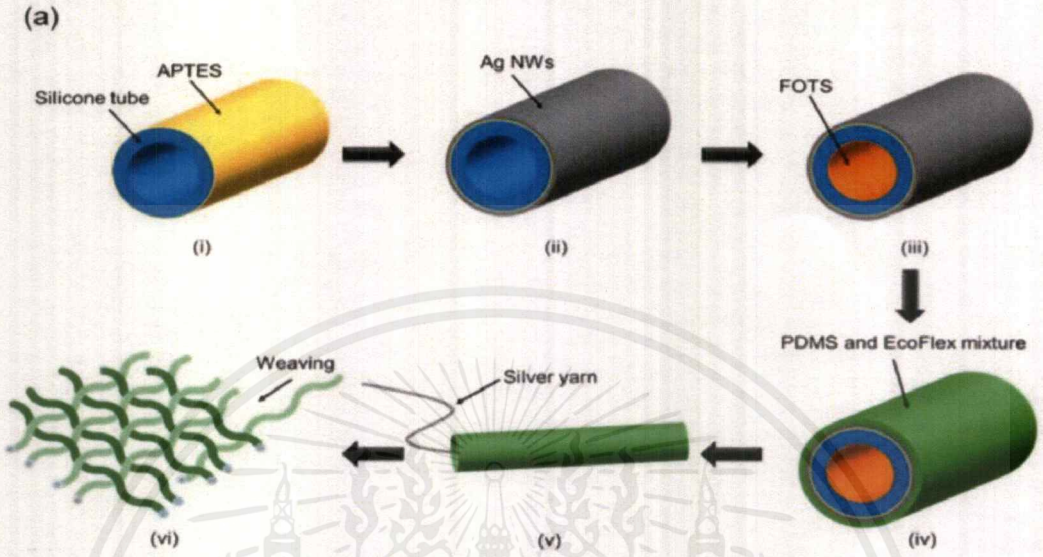

Figure 2.3 Fabrication of multifunctional woven structuer [28].

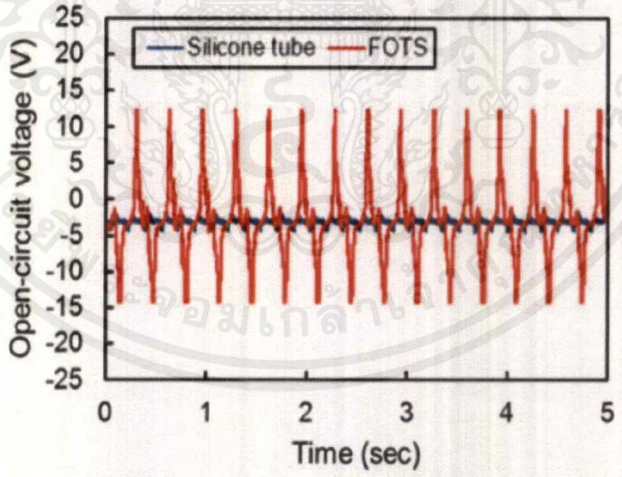

Figure 2.4 Real time profiles of open-circuit output voltages measured at frequency of 3 Hz with vertical force of 10 N with and without 2H perfluorooctyl-trichlorosilane (FOTS) coating [28].

Figure 2.4 shows the output properties of the prepared single functional thread when it is pressed and released repeatedly by a stamp with 10 N of pressing force. The actuation frequency was 3 Hz. The open-circuit output voltage was 2.3 V without the FOTS coating. However, by coating the inner surface of the tube with FOTS, they

obtain an output of 27.7 V, which is 12 times greater than the output without the FOTS coating, because FOTS, which is composed of fluorine atoms, provides a higher electron affinity compared to a bare silicone surface.

In our work we interested to add the allotrope and functionalize of carbon due to in the example of previous work they show increasing trends of the output performance by add or coat with it, so we combine the allotrope carbon (graphitic carbon nitride, graphite fluorinated) with PDMS to be a composite PDMS based for increase the output performance of triboelectric nanogenerator.

2.4 Improvement output performance of the TENG

There are numerous ways to improve the output of the TENGs including

2.4.1. Structure designs

The first way is to design a suitable device for energy harvesting from the desired source. TENGs can convert various types of mechanical energy from the environment into electricity, using the triboelectric effect and electrostatic induction. Four fundamental modes have been developed including vertical contact - separation mode, in – plane sliding mode, single electrode mode and free standing triboelectric-layer mode. Each mode has distinct structural features and advantages. The vertical contact – separation mode is suitable for harvesting cyclic motion, intermittent impact and vibration based on a periodic contact and separation of two contact surfaces. It offers various advantages, such as simple structure, excellent robustness and high instantaneous power density. The in-plane sliding mode has several advantages over the vertical contact- separation mode because its triboelectric effect is stronger than the contact effect. it is suitable for harvesting energy from planar motions and rotation. The single electrode mode has only one working electrode, and thus can harvest energy from an object moving freely. Finally, the free-standing triboelectric layer mode can conveniently harvest energy from the sliding or contact separation motion.

2.4.2. Selection of materials

The second way is the selection of the suitable materials. Almost all materials have triboelectric effect when paired with another metal, polymer, silk and even wood. All these materials can be candidates for fabricating a TENG. However, the ability of any one material to gain or lose electrons depends on its polarity. A large difference in polarity between two materials is increases the surface charge density. Therefore, many researchers aim to choose two materials that have a large separation in the triboelectric series. In addition, the surface morphology of materials can be modified by physical techniques to create different nano- or microstructures, such as strips, cubes and pyramids, which enhance the contact area. Moreover, the surface charge

density of materials can be increased by chemical techniques, such as ionized air injection or surface functionalization with various molecules, nanotubes, nanowires or nanoparticles.

Polydimethylsiloxane (PDMS) is a polymeric organosilicon compound that has been widely used as a negative triboelectric material. It is only slightly less negative triboelectric material than poly-(tetrafluoroethylene) (PTFE) in the triboelectric series. However, PDMS is more commonly used than PTFE, due to its flexibility, transparency and ease of modification. In addition, the cured PDMS has a hydrophobic property which makes the electrical output of a TENG less sensitive to humidity.

Many researchers improved PDMS properties by embedding various materials, such as piezoelectric materials, e.g. polyvinylidene fluoride (PVDF), Barium titanate ($BaTiO_3$), conductive materials (i.e., Carbon nanotubes (CNTs), Graphene, liquid metal, and ionic liquid) and so on, in a polymeric phase. These not only enhance the surface electrification, but also the intrinsic properties can be improved.

For instance, graphene oxide (GO) is classified as a negative triboelectric material, due to free oxygen functional groups in the structure. The addition of GO in the PDMS phase led to unusual nonlinear electrical conductivity and a high dielectric constant [29]. Harnchana et al [30] employed GO solution to modify PDMS and improve its triboelectric properties. The PDMS/GO composites with different concentration of GO solution were fabricated into films by spin-coating, as shows in Figure 2.5. The output of the fabricated PDMS/GO TENG operated in a single electrode mode were measured, under periodical compressive force. As the GO concentration increased, the output voltage and current also increased, led to the highest output at 215 V and 6 $\mu A/cm^2$. In contrast with flat PDMS, the PDMS/GO films presented porous structures that can increase surface contact area in polymeric matrix. In addition, they also incorporated sodium dodecyl sulfate (SDS) into the GO/PDMS system to enhance the negative charges in the PDMS composite. Under optimum operating conditions, the PDMS/GO/SDS TENG can generate the highest output voltage and current at 438 V and 0.11 A/m^2. The outstanding performance of the PDMS/GO/SDS TENG would be beneficial for further development of powerful nano-generators integrated into wearable electronics and self-charging power cells.

Flexible electronics are an emerging technology for a wide variety of new applications, such as wearable electronics, flexible displays, and stretchable energy devices. To improve both stretch ability and electrical conductivity, many researchers have incorporated conductive materials into flexible substrates. Among them, 1D CNTs and 2D graphene have been commonly employed to fabricate flexible electronics, due to its good properties such as, electrical conductivity, and mechanical properties. Zhu ,et. al [31] improved PDMS prepolymer with tunable internal resistance by doping

a Multi-walled Carbon Nanotube (MWCNT) to fabricate a flexible TENG, which has beneficial application for wearable devices. The device consists of PDMS and PDMS/MWCNT layers. Then, the surface of PDMS/MWCNT films were pattered to increase the contacting area. The PDMS/MWCNT film at 2 wt% MWCNT with micro-pillar patterns had a higher voltage than sample without micro-pillar patterns. For the effect of MWCNT concentration, the prototype I with 10 wt% MWCNT produced higher output voltage than prototype II with 2 wt% MWCNT with 30 V and 25 V respectively, due to its higher dielectric constant.

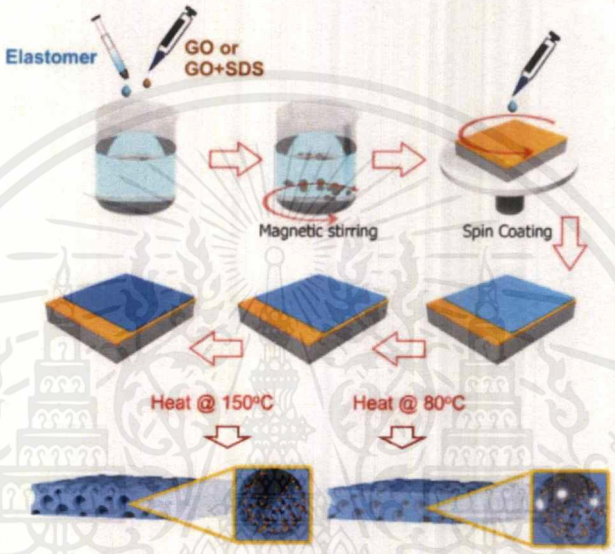

Figure 2.5 Schematic illustration of process flow for fabrication of PDMS@GO films using spin coating [31].

Fan ,et. al [32], also reported a stretchable porous nano-composite (PNC) based on a hybrid of a MWCNT network. The PNC was synthesized via templating. The MWCNTs and NaCl, as a sacrificial material, were directly mixed to PDMS prepolymer. Afterwards, the mixture was cast and polymerized on a suitable template. Then, the nano-composite was immersed in water to remove the NaCl particles, creating a 3D interconnected PDMS, as shows in Figures 2.6. a) and b).

a)

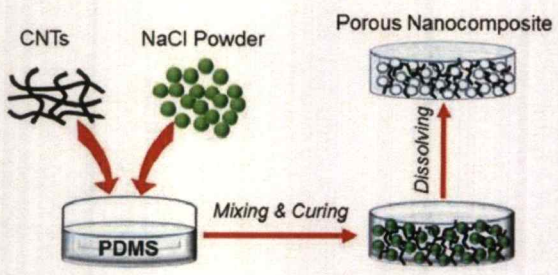

b)

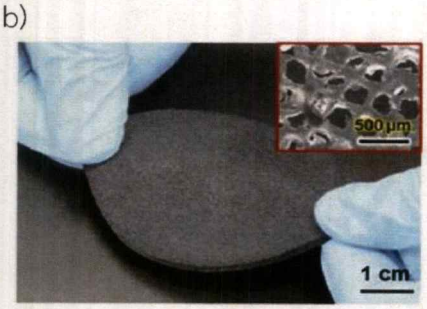

Figure 2.6 a) Diagram of the synthesis process and b) Photograph of an as-prepared round PNC (5 cm in diameter and 0.5 cm thick) [32].

When the CNTs concentration increased, the contact electrification between the CNTs and the PDMS matrix also increased and the formation of a conductive CNTs network to support the flowing of current could easily occur. In addition, the resistivity substantially decreased by more than two orders of magnitude, from 41 MΩm at 3 wt% to 0.43 MΩm at 5 wt%, as shows in Figure 2.7 e), caused by increasing of CNTs concentration. Moreover, the electrical output substantially increased with increasing of porosity, with more available inner surface area - see Figure 2.8. a). The effect of the dimensional PNC was also demonstrated, as the area of samples were increased in increment of 1 cm^2, the electrical output increased approximately linearly - see Figures 2.9. f) and g).

In summary, during the electrical measurement by using a completely novel energy harvesting device that generated the average voltage, 55V, and current, 170 nA. The PNC successfully harvested foot pressure and powered commercial LEDs. This approach provides a promising flexible power supply for wearable electronics.

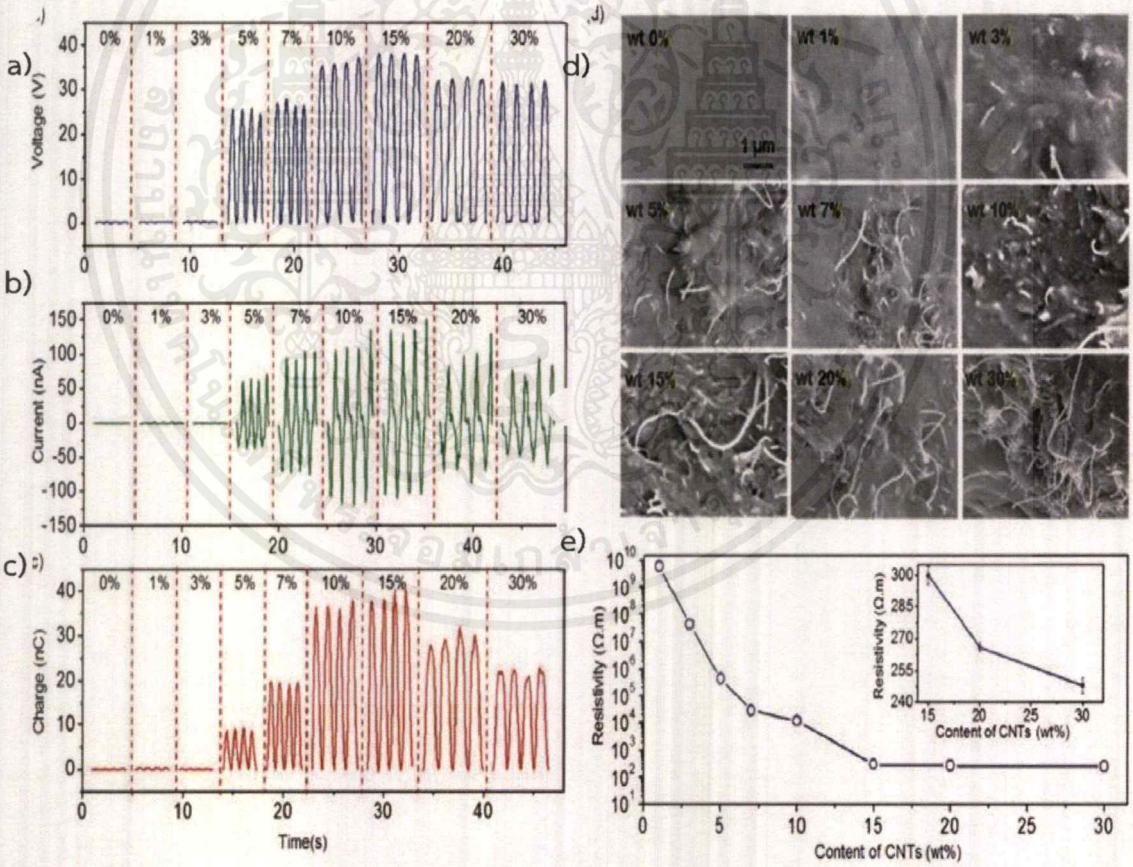

Figure 2.7 The effect of the CNTs content on the electrical output. The measured a) V_{OC}, b) I_{SC}, and c) charge output of the PNC as the CNTs content was varied from 0 to 30 wt% at a cycled compressive force of 40 N. d) SEM images of the inner surface morphology of the PNC and e) the resistivity with changing CNTs content [32].

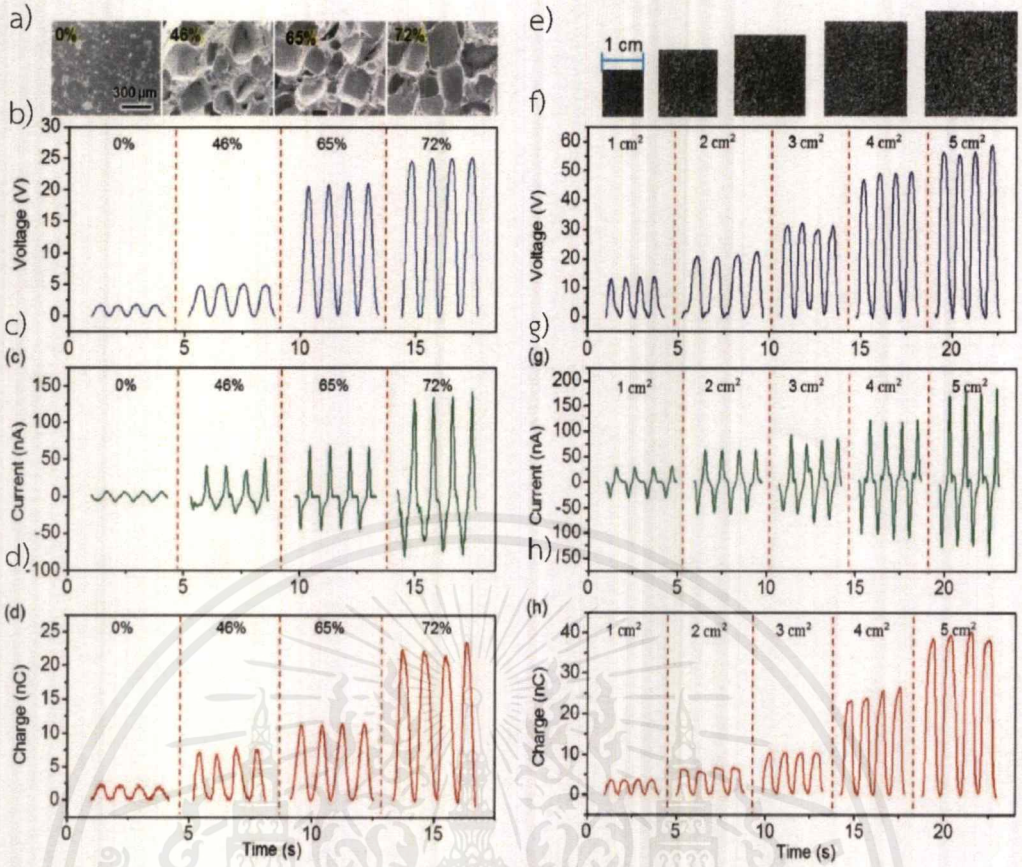

Figure 2.8 The effect of the porosity and the dimensions on the electrical output. a) Cross-sectional views of PNC samples with porosities ranging from 0% to 72%. The corresponding b) V_{oc}, c) I_{sc}, and d) charge output of the PNCs with different porosities. e) Photographs of the PNC samples with different lateral areas ranging from 1 to 5 cm^2. The corresponding f) V_{oc}, g) I_{sc}, and h) charge output of the PNCs with different lateral areas.[32]

2.4.3. Fabrication of porous PDMS

Many researchers have found various methods to fabricate porous PDMS, such as 3D printing, phase separation, templating, and so on, for applications in flexible conductors, energy generators, adsorbents, oil/water separators, biomedical scaffolds, etc.

For instance, Duan et al [33] used 3D printing to prepare porous PDMS, which has ordered structure. Polylactic acid (PLA) was formed into a 3D porous template that was used to make the 3D porous PDMS by direct casting. Afterwards, the PLA template was removed by etching with dichloromethane. Then, the 3D porous PDMS was integrated with a CNT/graphene network to fabricate a stretchable strain sensor, as shows in Figure 2.9 a). For this method, the pore characteristics, such as geometry, size and distribution can be controlled. However, this method is slow, high cost and damages the environment with toxic organic solvents.

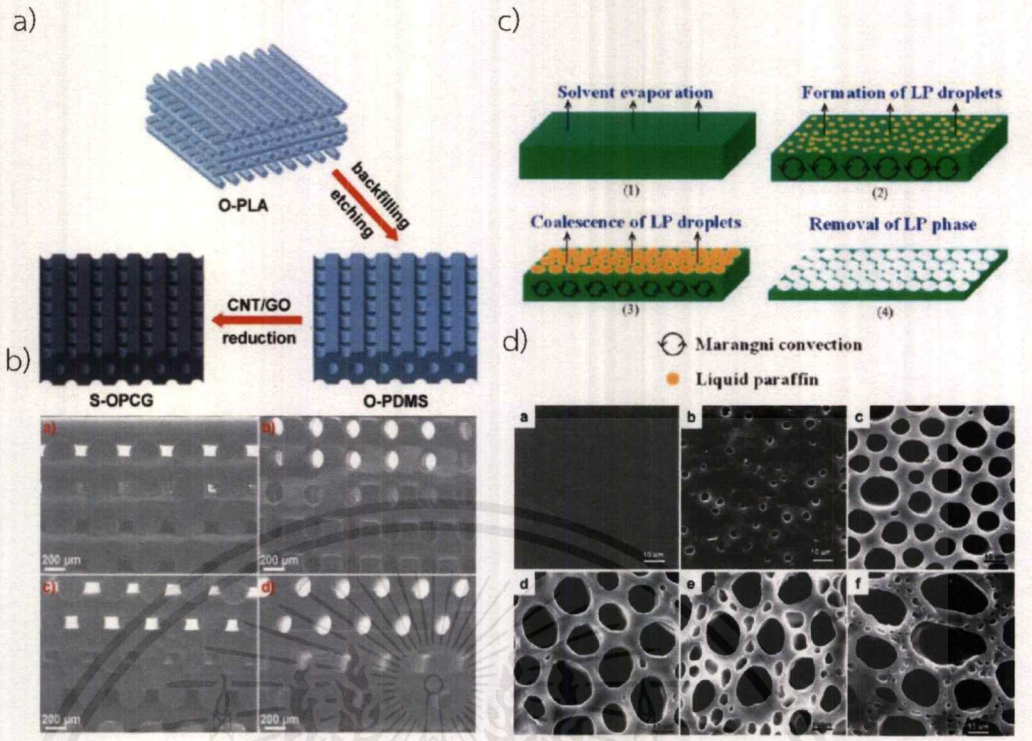

Figure 2.9 a) Schematic illustration of the split-level 3D porous PDMS/CNTs/graphene (S-OPCG) fabrication. b) Cross-section FE-SEM images of 3D porous PDMS and c) Schematic illustration of the microporous silicone rubber membrane fabrication and d) SEM images of the surface morphologies of the porous with various liquid paraffin concentrations[34].

Random porous structure was easily fabricated. Zhao et al [34] prepared porous silicone rubber membranes by using Evaporation-Induced Phase Separation (EIPS) method. The materials were either a mixture of liquid silicone rubber, liquid paraffin and hexane or liquid silicone rubber, liquid paraffin, hexane and span 80, which were prepared and cast into a mold. For this method, a liquid silicone rubber was dissolved in a mixture of a hexane and liquid paraffin. After the evaporating of hexane, the paraffin enriched droplets grow and coalesce, and the polymer solution was forced to separate into two phases: the polymer-rich phase and polymer-lean phase. Finally, the porous structure was formed by removing these paraffin enriched droplets, as shows in Figure 2.9. c). The average pore size and uniformity were controlled by the weight ratio of the liquid paraffin, as shows in Figure 2.9. d), casting temperature and thickness of the initial casting solution. The advantage of this method is that it scales up easily. However, using organic solvents in this method is unsuitable for health applications, oil-water separation and so on.

Templating, is likely a 3D printing, can fabricate random PDMS sponge structures. This method uses a sacrificial template material for fabricating a porous structure. Fabrication can be broadly described as follows: PDMS prepolymer and

curing agent were mixed together and cast in a sacrificial template. After polymerization, the sacrificial material was eliminated. So, a 3D interconnected PDMS can be obtained. Porosity and dispersion depend on the arrangement and nature of the template. Several materials, such as cube sugar or granulated sugar, salt, Citric Acid Monohydrate (CAM) or polymer particles can be used as a template.

For instance, Kang et al [35] used Polystyrene (PS) microspheres to fabricate PDMS sponges with well-ordered face-centered cubic structure of separated voids with a narrow size distribution. Especially, the pore size depends on the diameter of the adopted PS spheres. After polymerization, dimethylformamide was used to dilute PS spheres from cured PDMS.

Yu et al [36] prepared a porous PDMS sponge, for oil/water separation, by direct mixing CAM particles with PDMS prepolymer. After polymerization, the samples were immersed in ethanol for 6 h. to remove the CAM particles. In this method, the solvent is capable of wetting PDMS, and the template easily dissolved in the solvent.

For sugar and salt are commonly used as sacrificial template due to commercially availability, low cost, and eco-friendly preparation and no sophisticated laboratory equipment or hazardous solvent is required. For example, Choi et al [37] fabricated PDMS sponges for oil absorption by using different sizes of sugar particles. After the PDMS polymerization, these particles can be easily removed by soaking in water, creating a 3D interconnected PDMS, as shows in Figures 2.10 a) and b. The PDMS sponges were highly flexible and could be bent through a large degree without breaking and almost perfect recovering its original shape, when there were manually compressed - see Figure 2.11. c). However, the preparation required vacuum to infuse PDMS prepolymer into the templates. Therefore, many researchers have tried to improve the viscosity of PDMS prepolymer.

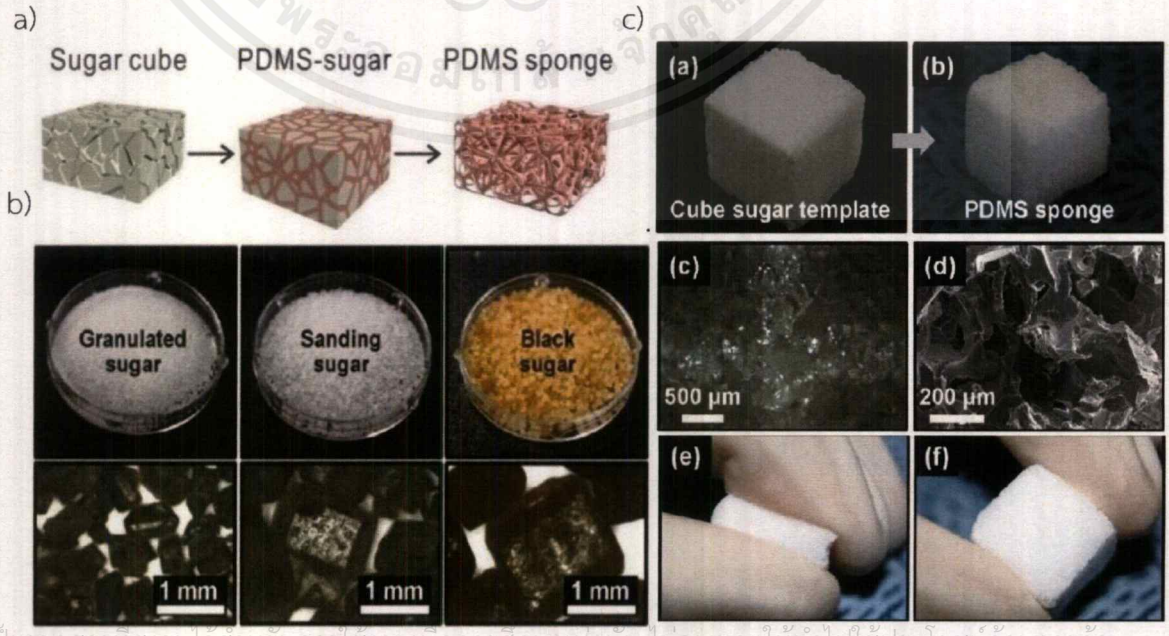

Figure 2.10 a) Schematic illustration of the fabrication process by using a cube sugar as the template. b) Photographs of sugar particles of different sizes and c) Photograph of (a) a commercially available cube sugar and (b) the as-replicated PDMS sponge. (c) Optical microscope image of the cross-sectional area of the PDMS sponge. (d) SEM image of the cross-sectional area of the PDMS sponge. (e) Manual compression to over 50% reduction in volume and (f) recovery to the original shape [37].

For instance, Zhang, et. al [38] reported a modified sugar leaching method to improve infusion of PDMS prepolymer. The p-xylene was used to dilute PDMS prepolymer and curing agent before mixing with sugar particles to fabricate the sponge, as shows in Figure 2.11. a). The p-xylene solvent decreased the viscosity of PDMS prepolymer so it could easily fill the cavities within the sugar particles and prevented the formation of bubbles, avoiding the requirement for vacuum, in contrast with the PDMS porous fabricated with a conventional sugar-template method. After polymerization and removal of the template and solvent, the resultant PDMS porous swollen, as shows in Figure 2.11. b). The main reason for the swelling of structure may be that the p-xylene solvent prevented cross-linking in PDMS. As a result, the structure could not support its own weight and collapsed.

Although porous PDMS has been successfully synthesized, the effect of sacrificial material, including the kind and size of particles, a solvent to dissolve template, as well as a solvent to dilute PDMS prepolymer, remains to be studied.

a) b)

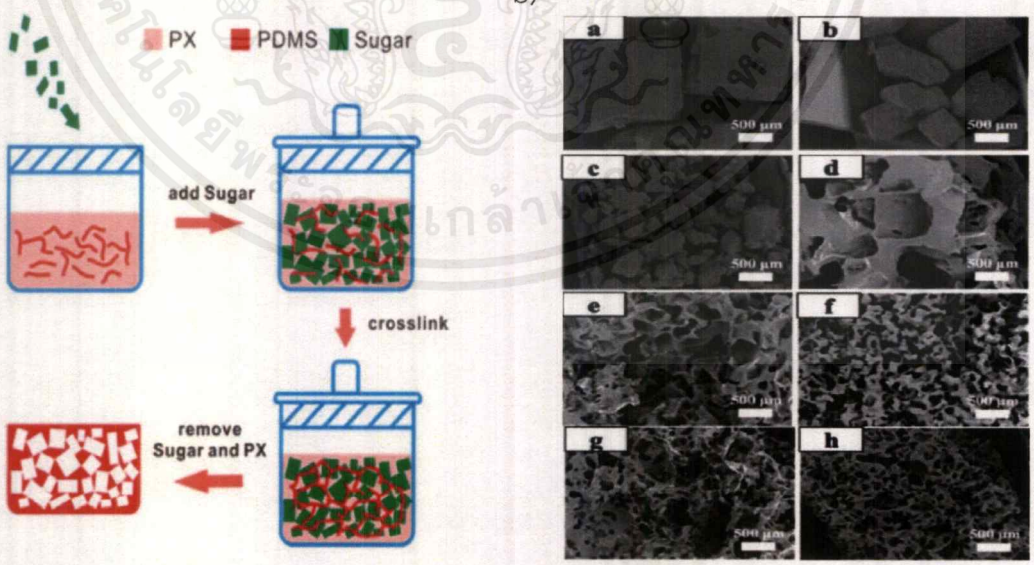

Figure 2.11 a) Schematic illustration for the preparation of PDMS oil absorbents via a sugar template technique. and b) SEM images of sugar particles of various sizes and PDMS oil absorbents [38].

For instance, Zhao et al [36] selected dimethicone as solvent to dilute PDMS prepolymer and NaCl particles were used as a sacrificial template, as shows in Figure 2.12 a). The porosity was controlled by varying the weight ratio of the PDMS prepolymer to dimethicone and the NaCl particle size. It exhibited excellent compressive and tensile properties, attributed to its interconnected 3D porous structure. No obvious change in the compressive stress–strain curves was observed after 100 compression cycles. In addition, no fracture or collapse of the sponge was observed during the testing. Nevertheless, the increasing of weight ratio of dimethicone solvent to PDMS prepolymer decreased the mechanical strength of obtained PDMS sponge.

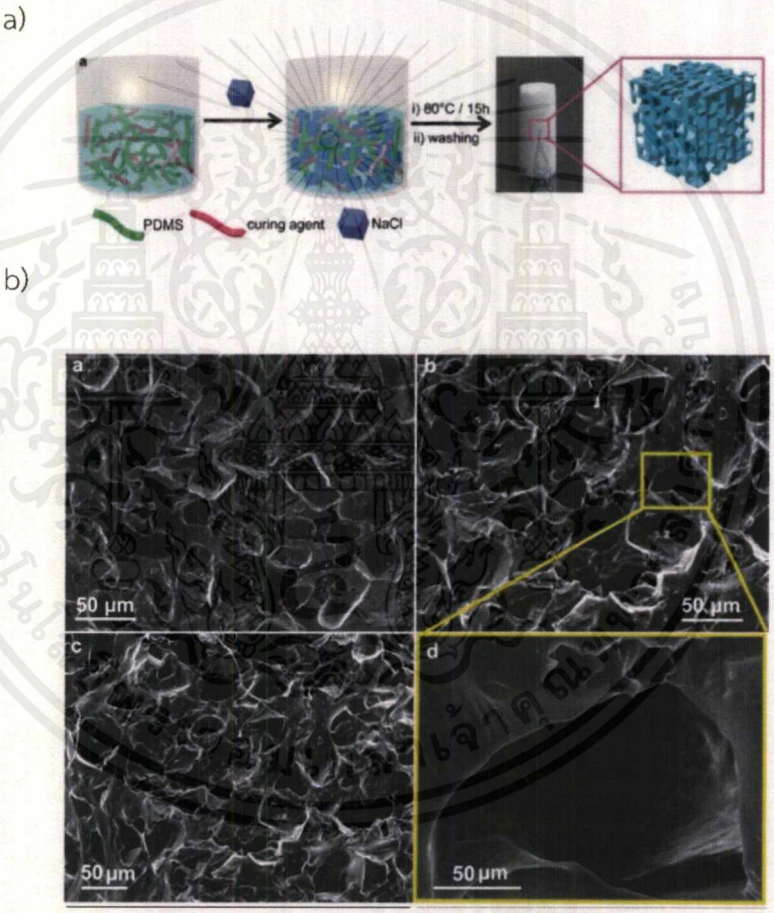

Figure 2.12 a) Schematic illustration for preparing the PDMS sponges, and b) SEM images of the (a) PDMS 8# (b and d) PDMS 13#, (c) PDMS 2# sponges [36].

CHAPTER 3
EEPERIMENTAL PROCEDURES

In this research, we described (1) the fabrication process of the PDMS sponge by templating process. (2) the fabrication of the composite PDMS sponge by using several allotropes as composite materials and (3) the fabrication of the TENG.

3.1 Materials

1) Polydimethylsiloxane (PDMS) (Sylgard 184, Dow Corning Co.)
2) Cubes brown sugar (Orchid, Theparos Roong Ruang Co.)
3) Cubes white sugar (Orchid, Theparos Roong Ruang Co.)
4) Brown sugar crystals (Lin, Thai Roong Ruang Sugar Group)
5) White sugar crystals (Lin, Thai Roong Ruang Sugar Group)
6) Monosodium glutamate (MSG) (Ajinomoto, Ajinomoto Co., Inc.)
7) Salt crystals (Prung Thip, Thai Refined Salt Co., ltd.)
8) Graphite, fluorinated, polymer (>61 wt% F) (372455-5G, Sigma Aldrich Co.)
9) Graphitic carbon nitride (g-C_3N_4)

3.2 Glasswares and equipments

1) Beaker size 150 and 1000 ml.
2) Spatula Stainless
3) Glass rod
4) Dropper
5) Mold (5 cm (height) x 7.6 cm (width) x 7.6 cm (length))
6) Ultrasonic Processor (VC750, Sonics & Materials, Inc.)
7) Circulating Aspirator (WJ-15 100V, SIBATA SCIENTIFIC TECHNOLOGY LTD.)
8) Oven (Memmert GmbH + Co.KG)
9) Hot magnet stirrer (C-MAG HS7, IKA Works GmbH & Co.)

3.3 The fabrication

3.1 Fabrication of the PDMS sponge

Figure. 3.2. Schematic illustrations of the fabrication process of PDMS sponge. The different type of particles (i.e., cube brown sugar, cube white sugar, brown sugar crystals, white sugar crystals, monosodium glutamate crystals and salt crystals) were added into each mold as sacrificial templates. The mixture of PDMS prepolymer and curing agent that were mixed in a ratio of 10: 1 by weight was directly added into each template. For the mass ratio of the compositions were controlled, as shows in table 1 at 0 wt% of a dispersed phase. Then, the PDMS prepolymer/curing agent were hand mixed together for 5 min. and raped in order to pack the particles and remove the

bubbles, which are occur in mixing process for 10 min. Moreover, to ensure that there are no air bubbles remain in the mixture, it was placed in a vacuum desiccator for 1 h. After that, the mixture was cured in an oven for 2 h. at 70 °C to accomplish the polymerization.

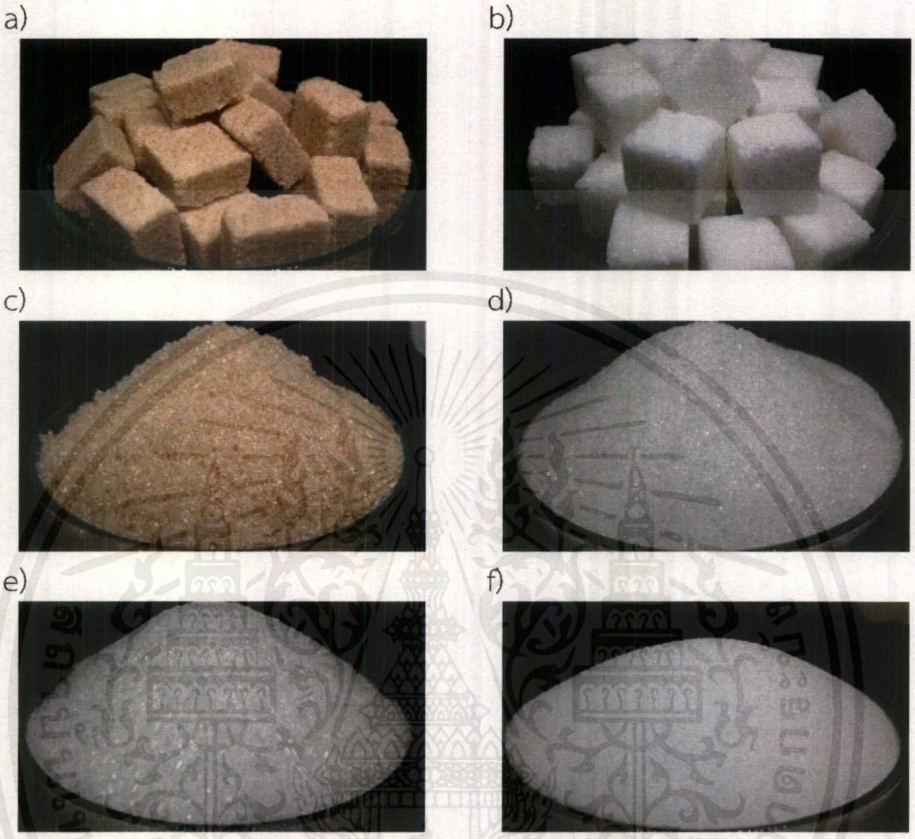

Figure 3.1 Photograph of the different type of particles for the templating. a) cube brown sugar, b) cube white sugar, c) brown sugar crystals, d) white sugar crystals, e) monosodium glutamate crystals and f) salt crystals

Afterward, the cured samples were cut into the square shape with the dimension is 30 mm x 30 mm and the thickness 10 mm. before the leaching in deionized water at 100 °C for 3 days. During the heating process, the water was replaced every 1 h. to make sure that the sacrificial templates was eliminated. Finally, the PDMS sponges were dried in an oven at 100 °C for 1 day.

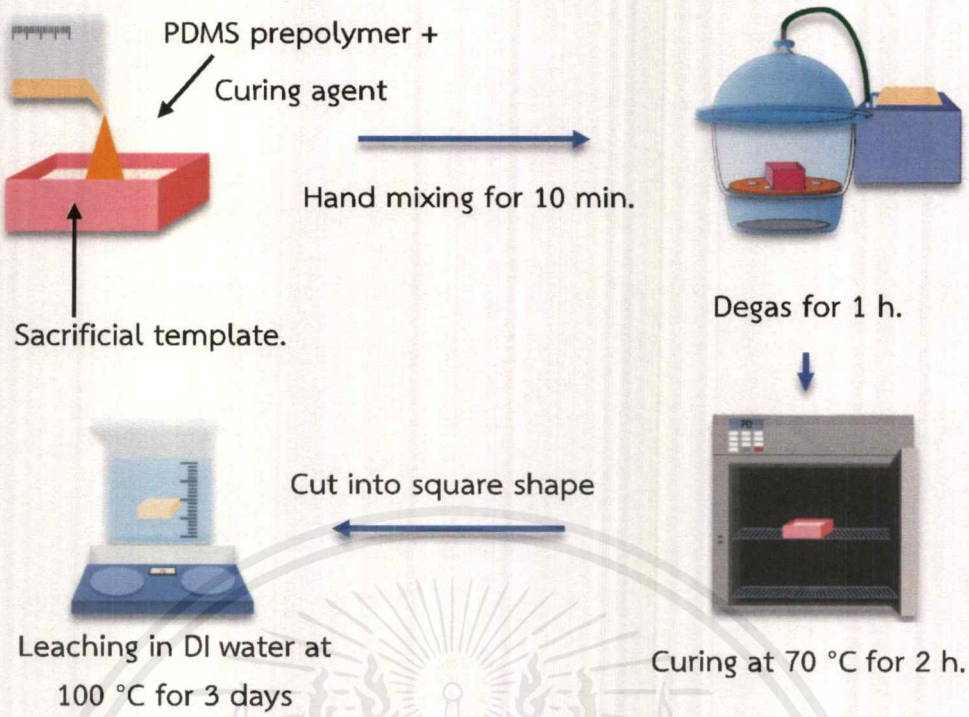

Figure 3.2 Schematic illustrations of the fabrication process of PDMS sponge by templating.

3.2 Fabrication of the composite PDMS sponge

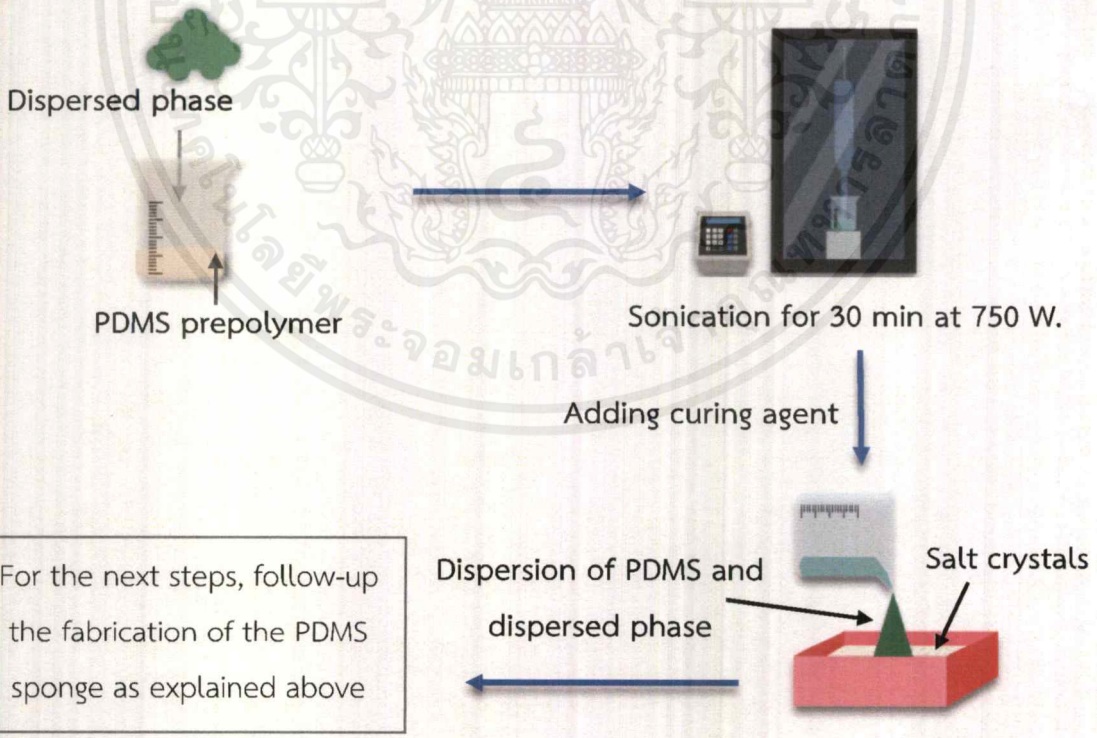

Figure 3.3 Schematic illustrations of the fabrication of composite PDMS sponge by using salt crystals as a sacrificial template.

In this study we fabricated the composite PDMS sponge by using the Graphite fluoride and Graphitic carbon nitride (g-C_3N_4). we used the same method as explained above to fabricate each composite PDMS sponge.

Figure. 3.3. schematic illustrations of the fabrication of composite PDMS sponge, PDMS prepolymer and dispersed phase were mixed by sonication for 30 min. at 750 W. to obtain well-dispersion. The weight ratio of between the PDMS prepolymer and dispersed phase, as listed in Tables 3.1 and 3.2. After the dispersion was cooled at room temperature, a curing agent is added and mixed together by hand. Then, the dispersion was directly added into the salt particles. For the next steps, follow-up the fabrication process of the PDMS sponge as explained above

Table 3.1 The weight ratio of g-C_3N_4 for the composite PDMS sponge fabricating.

wt%	g-C_3N_4 (g.)	Template (g.)	PDMS (g.)	Curing agent (g.)
0	-	46.0426	20.6765	2.0676
1	0.2068	46.0426	20.6765	2.0676
3	0.6203	46.0426	20.6765	2.0676
5	1.0338	46.0426	20.6765	2.0676
10	2.0676	46.0426	20.6765	2.0676

Table 3.2 The weight ratio of Graphite Fluoride for the composite PDMS sponge fabricating.

wt%	Graphite Fluoride (g.)	Template (g.)	PDMS (g.)	Curing agent (g.)
0	-	46.0426	20.6765	2.0676
10	4.1353	46.0426	20.6765	2.0676
20	8.2706	46.0426	20.6765	2.0676
40	8.2706	46.0426	20.6765	2.0676
60	12.4059	46.0426	20.6765	2.0676

3.4 Fabrication of the TENG.

A typical structure of TENG is schematically shows in Figure. 3.4. The device consists of two layers a sponge and metal plate that based on contact separation mode to harvest energy from the foot pressure. In the fabrication, Polymethyl

methacrylate (PMMA) was selected as material for both of substrates due to its decent strength and light weight. One of the plates of substrate on the lower side, a Kapton tape as an insulator and Cu tape as an electrode are deposited. Then, the PDMS sponge was adhered on Cu tape. For the other plate of substrate, a Kapton and Cu tape were also deposited on the surface of substrate and a non-modified Al plate, which acts as both contact surface and electrode was adhered on Cu tape. Both the substrates were connected by four springs installed at the corners, top side is lift up to appear a gap between two surfaces of a sponge and metal plate.

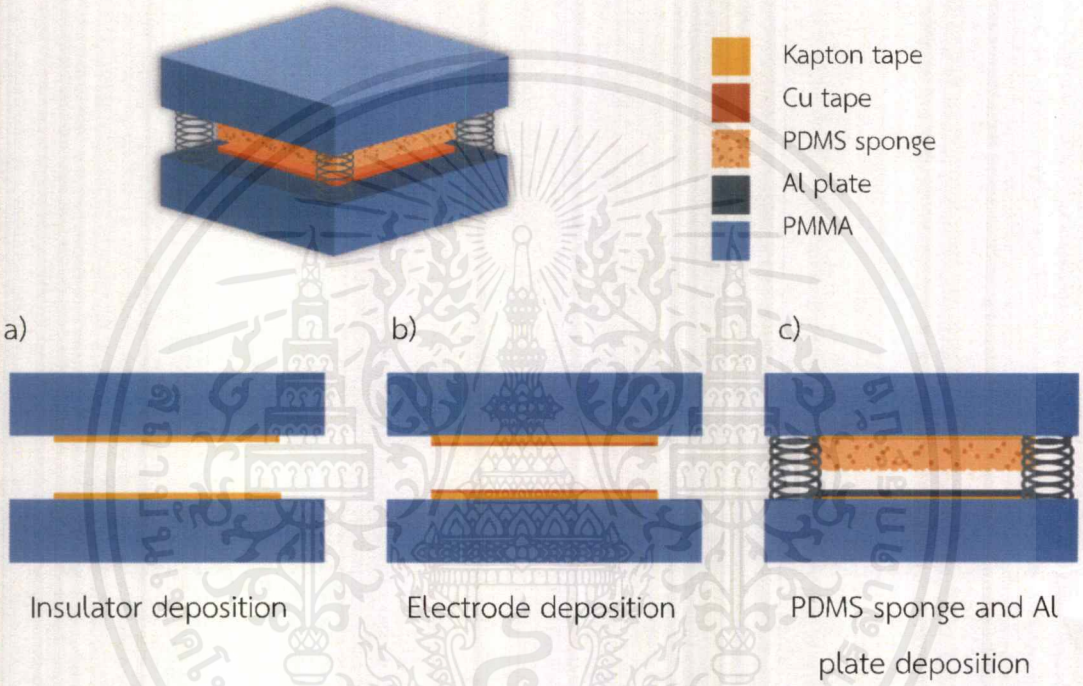

Figure 3.4 Illustration of the fabrication the TENG based on contact separation mode describe to the materials selection and device structure, a) and b) a Kapton and Cu tape as an insulator and electrode respectively were deposited and c) PDMS sponge and Al plate as a contact surface were adhered.

3.5 Characterizations

Raw materials as a sacrificial template: The close-up image was investigated using an Optical microscope and Scanning Electron Microscope (SEM, QUANTA 250, FEI) at an accelerating voltage of 15 kV. Infrared spectra were recorded using a Fourier Transform Infrared spectroscopy (FT-IR, FTIRSPECTRUM GX) at a spectral range 400 – 4000 cm^{-1}.

Raw materials as a dispersed phase: The morphology was investigated using SEM (QUANTA 250, FEI) at an accelerating voltage of 15 kV. Infrared spectra were

recorded using a FT-IR (FTIRSPECTRUM GX) at spectral range 400 – 4000 cm^{-1}, Raman spectroscopy, and X-ray diffraction (XRD, (D8 Advance, Bruker AXS) was analyzed to investigate the characteristic materials.

Fabricated sponge: The morphology was investigated using SEM (QUANTA 250, FEI) at an accelerating voltage of 15 kV. Infrared spectra were recorded using a FT-IR (IRTracer-100, SHIMADZU) at spectral range 700 – 4000 cm^{-1} and XRD (D8 Advance, Bruker AXS) was analyzed to investigate the characteristic materials. The surface wettability of the sponges was measured using contact angle analysis (OCA20, DATAPHYSICS) by water droplets of 5 μL in volume. The compressibility was measured Universal testing machine (LR5K, LLOYD) by applying constant compressible force of 300 N. The dielectric property measurements were analyzed by using LCR analyzer (HP – 4284, HEWLETTE PACKARD)

3.6 Electrical characterization

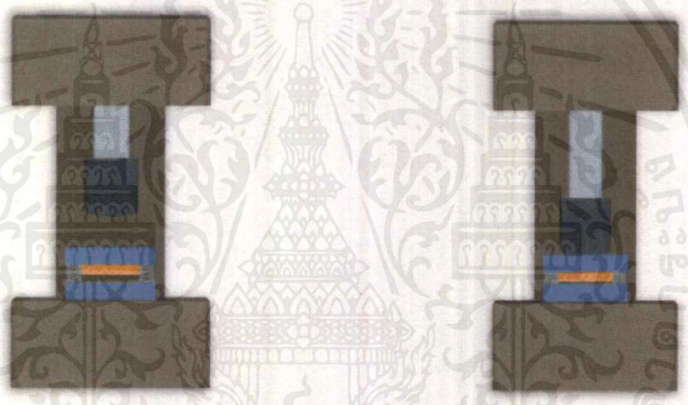

Figure 3.5 The force applying setup and the working principle

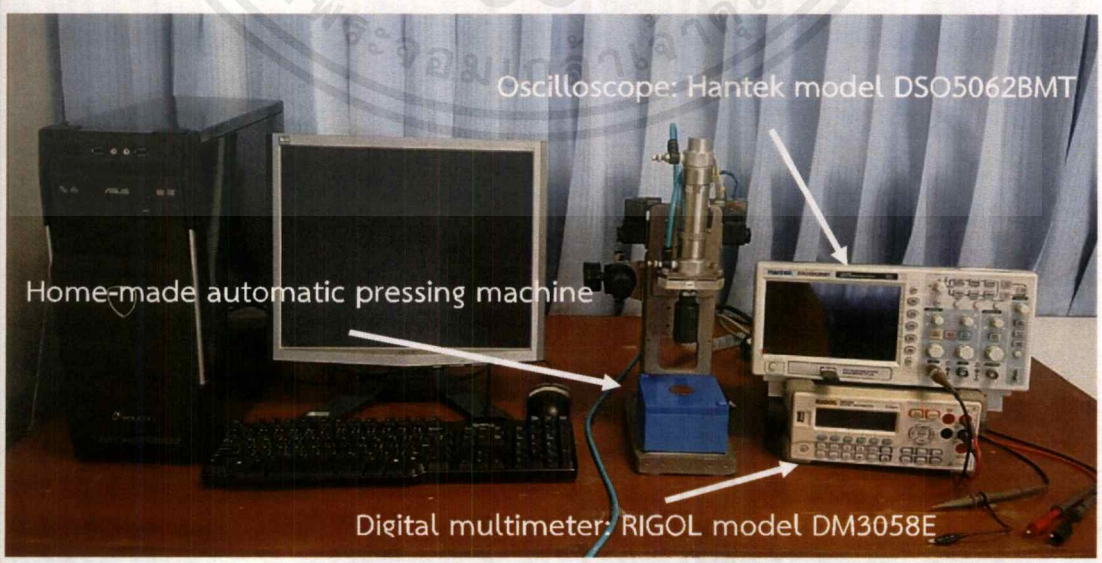

Figure 3.6 The force applying setup and the output performance detector.

The research investigated the electrical characterization of the fabricated TENG. By measuring the output performance through the vertical contact separation mode. For the force applying setup as shows in Figure. 3.5. The connecting configuration that had a positive probe related to the Cu plate layer and a negative probe connected with the PDMS sponge layer.

During the electrical measurement, a vertical force of 247 N was periodically loaded onto the TENG and reverted to the original position at a frequency of 1.5 Hz. Then, the open circuit voltage (V_{oc}) and short circuit current signal (I_{sc}) were detected. Both the force applying, and the detected output performance were controlled by a programmable logic controller (PLC).

CHAPTER 4
RESULTS AND DISCUSSION

In this section, we reported and discussed in (1) the fabricated PDMS sponges and composite PDMS sponge. (2) the characteristic analysis of these samples comprising the morphology, composition, mechanical properties include the manual testing, compression testing and contact angle measurement, and electrical properties include the output voltage and current performance and dielectric property measurement.

4.1. The fabricated PDMS sponge by templating

In this work we use various type of particles, which have different size and shape, as sacrificed template. We expected it can form interconnected 3D porous structure and provide a different porosity of PDMS sponge.

4.1.1 Characterization

4.1.1.1 Scanning electron microscope (SEM) measurement.

Investigation the morphologies of sacrificed templates by SEM and measured templates and porous size by digital camera.

a)

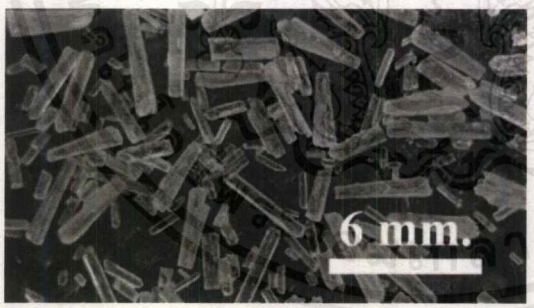

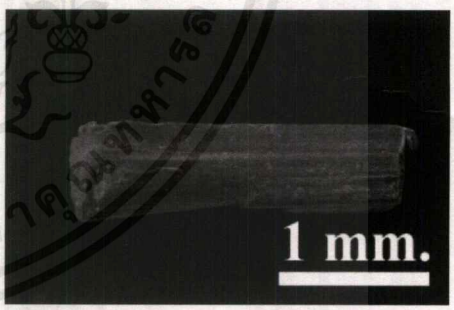

b)

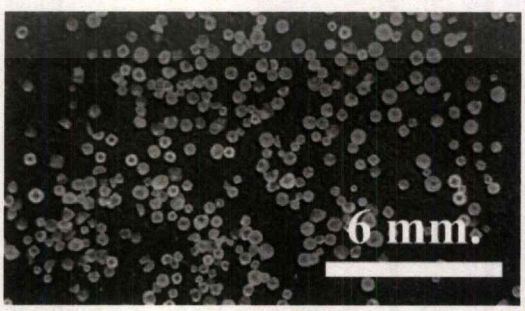

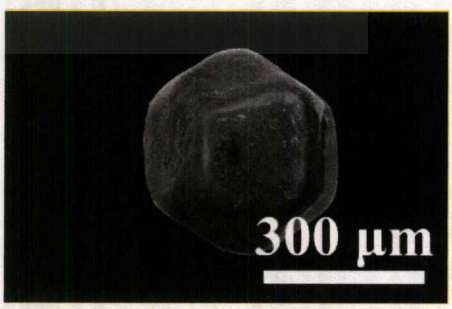

c)

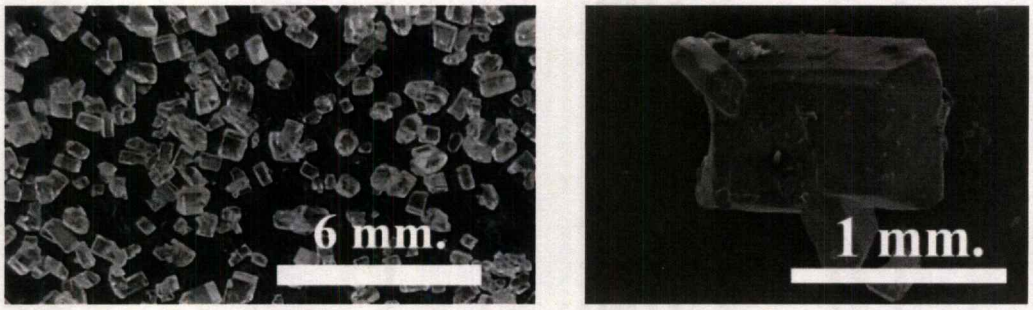

d)

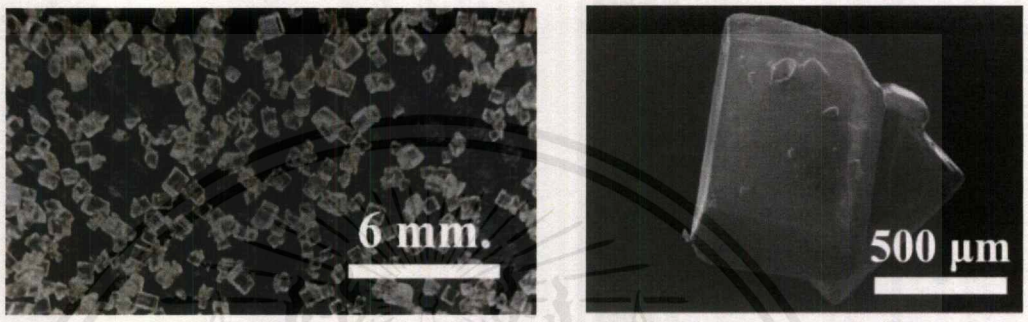

Figure 4.1 SEM micrograph show shape and size distribution of a) MSG, b) salt, c) white sugar and d) brown sugar by digital camera on left and SEM on the right.

The morphology of monosodium glutamate is rod shape (Figure 4.1 a)) and aspect ratio is 3.55 : 1, in morphology and size of PDMS sponge by monosodium glutamate template is 2.77 : 1 (Figure 4.2 a)). Average size of salt particle (Figure 4.1 b)) is 0.3654±0.0919 mm. and porous size in PDMS sponge by salt template (Figure 4.2 b.). is 0.3654±0.0919 mm. Rectangle shape white sugar template (Figure 4.1 c)) has aspect ratio is 1.55 : 1 and PDMS sponge from white sugar template (Figure 4.2 c)) has a porous size aspect ratio is 1.59 : 1. Rectangle shape of brown sugar template (Figure 4.1 d)) has aspect ratio is 1.27 : 1 and PDMS sponge from brown sugar template (Figure 4.2 d)) has a porous size aspect ratio is 1.66 : 1. The unspecified shape of cube white sugar and cube brown sugar templates (Figures 4.2 e) and f)) provide the fine and various porous shape of PDMS sponge. Summarize that the result of SEM indicated that all sacrificed template (monosodium glutamate, salt, white sugar, brown sugar, cube white sugar and cube brown sugar) provide different porous shapes of PDMS sponges and salt sacrificed template that provide a good size distribution of porous in PDMS sponge.

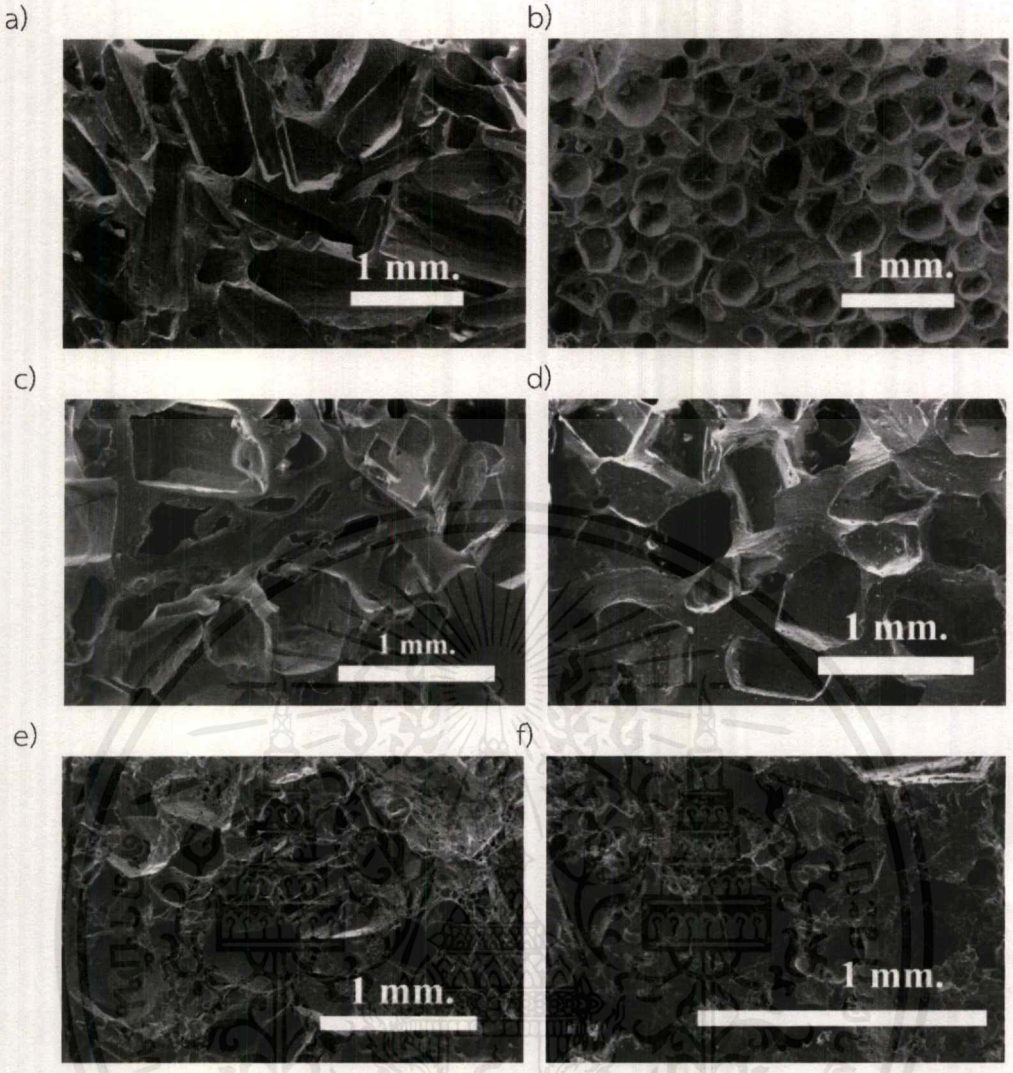

Figure 4.2 SEM micrograph show shape and size distribution of pore in sponge PDMS by using sacrificial templates a) MSG, b) Salt, c) White sugar, d) Brown sugar, e) Cube white sugar, f) Cube brown sugar by SEM.

a) PDMS sponge from Cube Brown Sugar template (CBS-PDMS sponge)

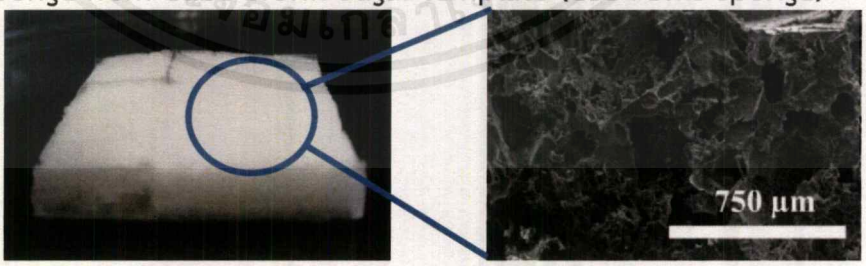

b) PDMS sponge from Cube White Sugar template (CWS-PDMS sponge)

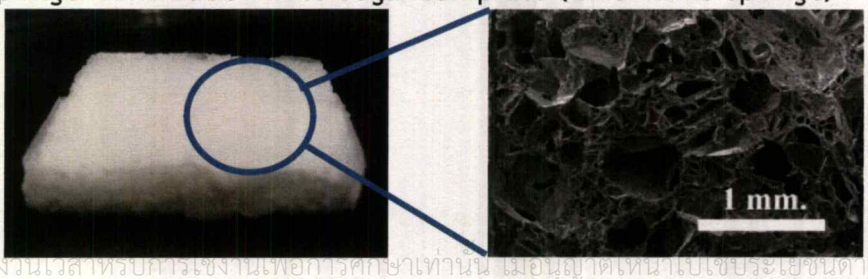

c) PDMS sponge from Brown Sugar template (BS-PDMS sponge)

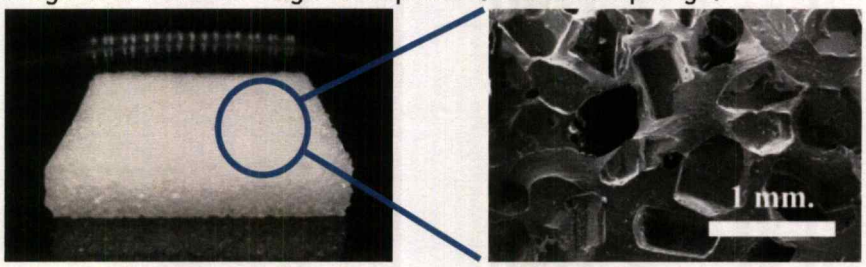

d) PDMS sponge from White Sugar template (WS-PDMS sponge)

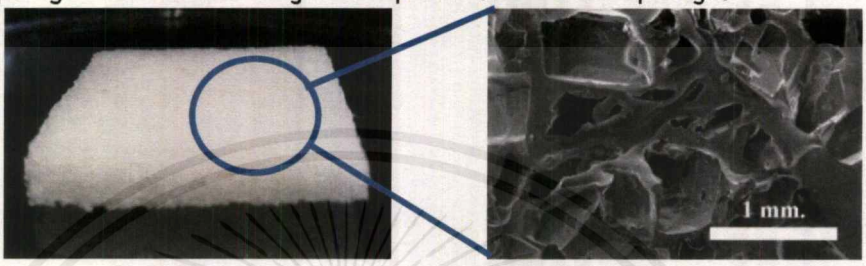

e) PDMS sponge from Monosodium glutamate template (MSG-PDMS sponge)

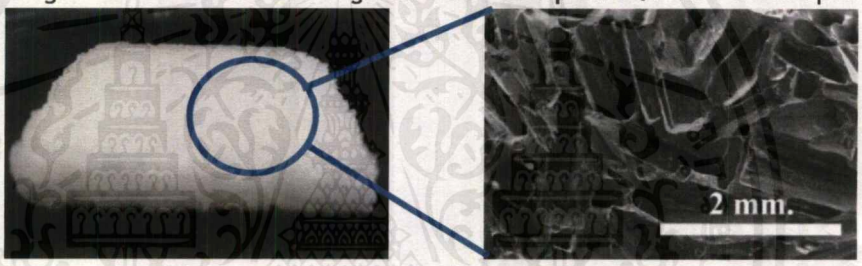

f) PDMS sponge from salt template (Salt-PDMS sponge)

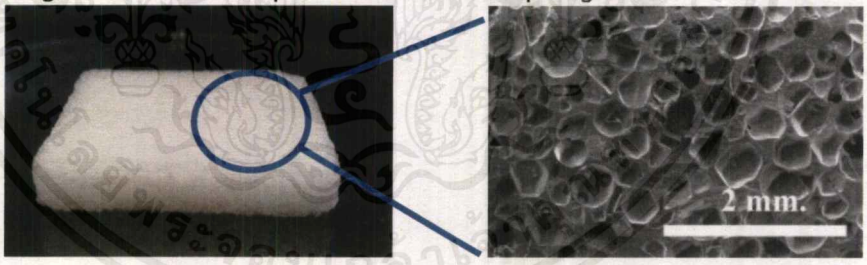

Figure 4.3 Photograph and SEM images shows morphologies of the obtained PDMS sponges that were fabricated by different type of particles as a template.

Following with the previous experimentation, the PDMS sponges were fabricated by using different morphological types of commercial particles. Close-up views from digital camera (Left, Figure 4.3) and SEM (Right, Figure 4.3) show that the obtained PDMS sponges consist of a porous and interconnected three-dimensional framework. It is inferred that the porosity of each sponge obviously is consistent the structure of the template and hence can adjust a morphology of sponge by selecting a particle, which was used as a template.

4.1.1.2. Fourier transform infrared spectroscopy (FT-IR) measurement.

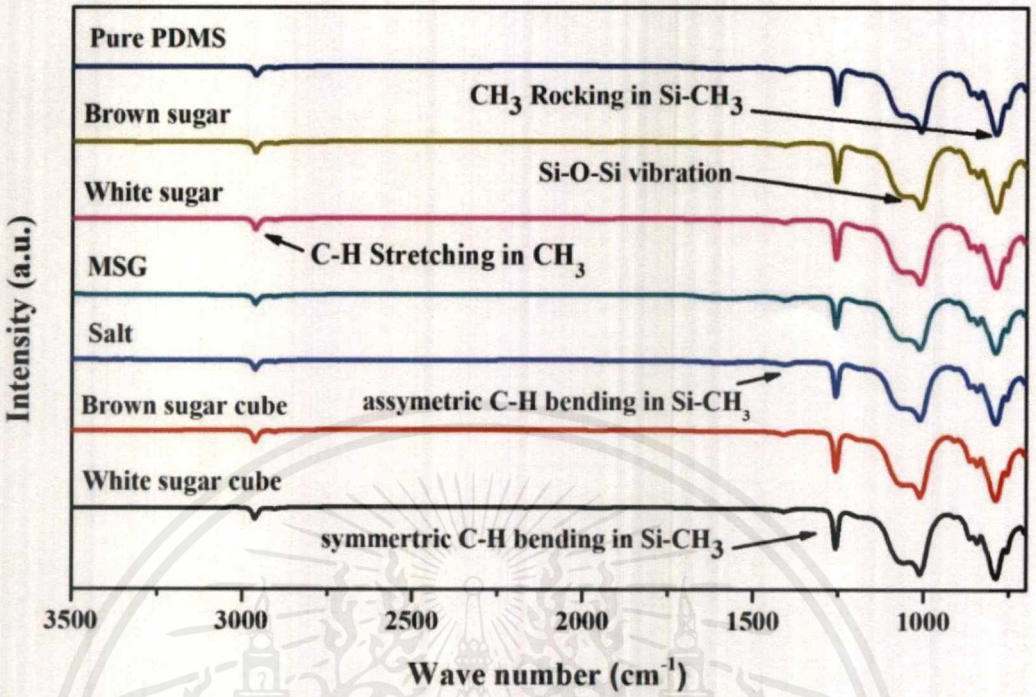

Figure 4.4 Infrared spectra of PDMS sponge by using sacrificial templates were recorded using a FT-IR (IRTracer-100, SHIMADZU) at spectral range 700-4000 cm^{-1}.

The infrared spectra, as show in Figure 4.4. The characteristic peak of PDMS show multiple absorption bands in the region 700 – 3500 cm^{-1}, which correspond to stretching and bending vibrations of PDMS. Of these, peak of around 1010 cm^{-1} and shoulder at 1070 cm^{-1} corresponding to Si-O-Si vibration , the peak around of 1257 cm^{-1} ,1409 cm^{-1} has been attributed to the deformed vibration of CH_3 groups. Peak at around 786 cm^{-1} assigned for rocking vibration of CH_3 groups and the peak around of 2961 cm^{-1} is related to the stretching vibration of C-H band [39], respective. From FTIR spectrum in Figure 4.4. that demonstrate all templates can use for fabricate the PDMS sponge due to do not have a bonding between two matrixes that described by not found the bonding peak between templates and PDMS.

4.1.1.3 Contact angle measurement

In principle, the surface charge that was generated through triboelectric effect depends on the ambient relative humidity. The output voltage and current performance of the TENGs, which previously were reported, generally decrease as the ambient relative humidity increase.[40, 41]

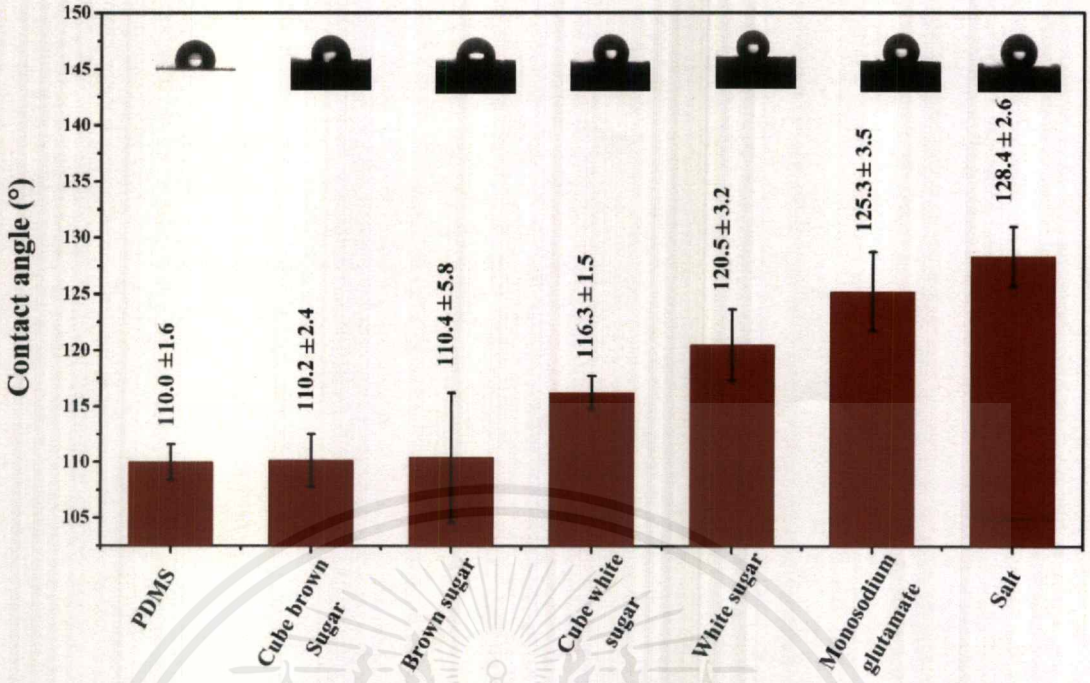

Figure 4.5 Contact angle on the Flat and Sponge PDMS surfaces with optical images of water droplets.

However, PDMS is inherently hydrophobic surface because it has methyl groups that are introduced into all side chains and both ends cause its surface energy is low. Moreover, the presence of porosity on surface of PDMS sponge can increase the hydrophobic property due to the upward force generated by the air inside the pores, which lifted water droplets.[42] Demonstrated by the surface wettability measurement, water was dropped on the surface of each sample, as shows in Figure 4.5, the PDMS flat still exhibits hydrophobic surface. For the PDMS sponges, which were formed by different types of templates, exhibit different surface wettability. The contact angles of CBS-PDMS sponge, CWS-PDMS sponge and CBS-PDMS sponge show value in range between 90 to 120 that are hydrophobic surface as the PDMS flat. For the WS-PDMS sponge, MGS-PDMS sponge and Salt-PDMS sponge surfaces show the contact angle between 120 to 150 that is range of ultra hydrophobic surface. Among them, the Salt-PDMS sponge shows the highest hydrophobicity at 128°.

4.1.2 Mechanical measurement

4.1.2.1 Manual testing

Table 4.1 Photograph the PDMS sponges that were fabricated by different type of template and Manual testing

Templates	Sponge PDMS	Manual testing	
		Bending	Twisting
-	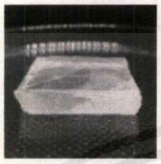	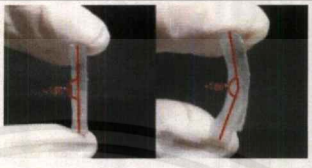	
Cube brown sugar		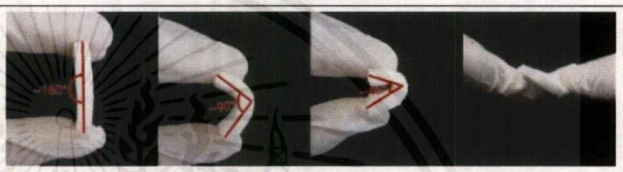	
Cube white sugar		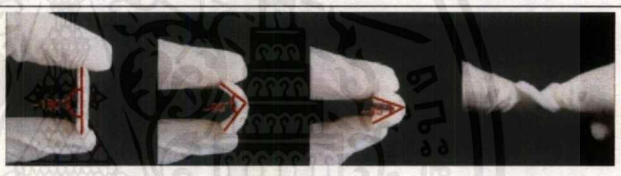	
Brown sugar		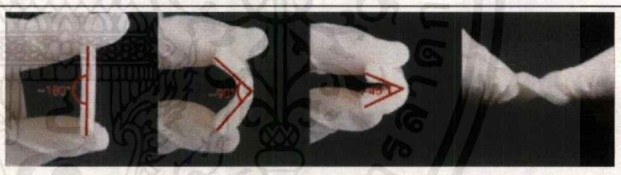	
White sugar		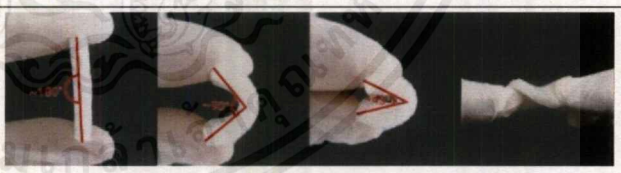	
MSG	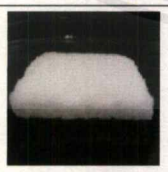	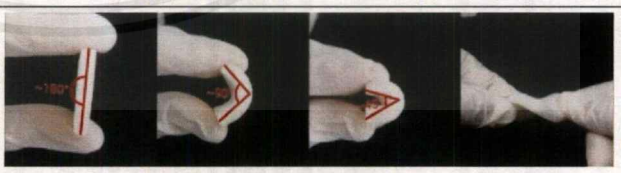	
Salt	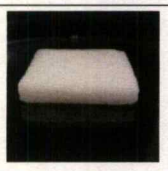	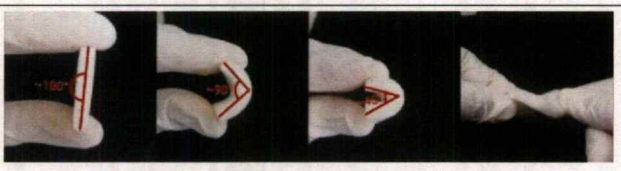	

These PDMS sponges exhibit a structural flexibility, as shows in Table 4.1, it can be bent over 45° from 180° and twisted by manual testing without breaking apart and

can almost perfectly recover its original shape abruptly. Meanwhile, the PDMS flat is not bent more over approximately 150° in same volume.

4.1.2.2 Compression testing

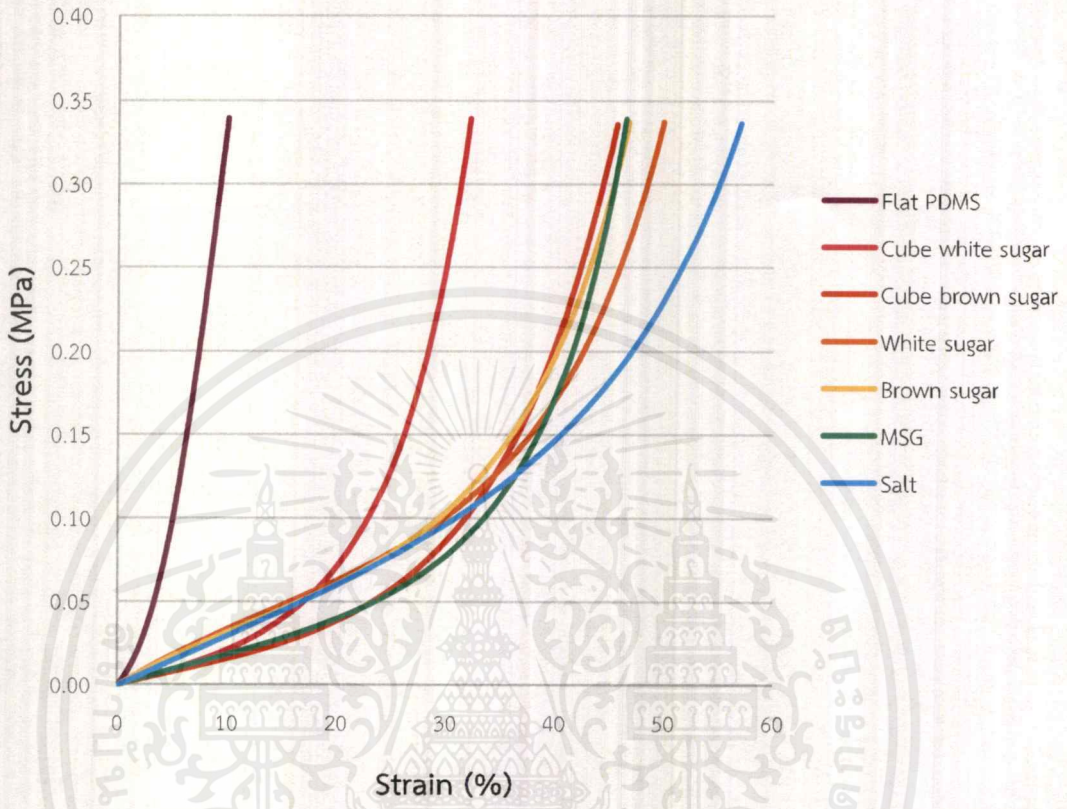

Figure 4.6 Stress – strain curves of the Flat and Sponges PDMS under constant-force compression at 300 N.

Compression testing was conducted to evaluate the displacement of the samples under applying external force. Its stress-strain curves under fixed vertical force at 300 N, as shows in Figure 4.6, with the stress led to 0.34 MPa, the strain (%) of the PDMS flat is about 10% of strain while each of the PDMS sponge can be compressed over 30% of strain. It can be clearly observed that the compliance value of the PDMS sponges are higher than the PDMS flat, as presents in Table A4.1 in APPENDIX A, it can be explained that the PDMS sponge exhibit mechanical softness that the PDMS flat. Among the PDMS sponges, the Salt-PDMS sponge is the highest mechanical softness, which is over 50% of compliance value.

These PDMS sponges can recover to its original volume after compressible force was released. This property is attributed to the flexible chemical chain of PDMS (-Si-O-) and the presence of porosity in matrix [43].

4.1.3 Electrical measurement

4.1.3.1 The output voltage and current performance

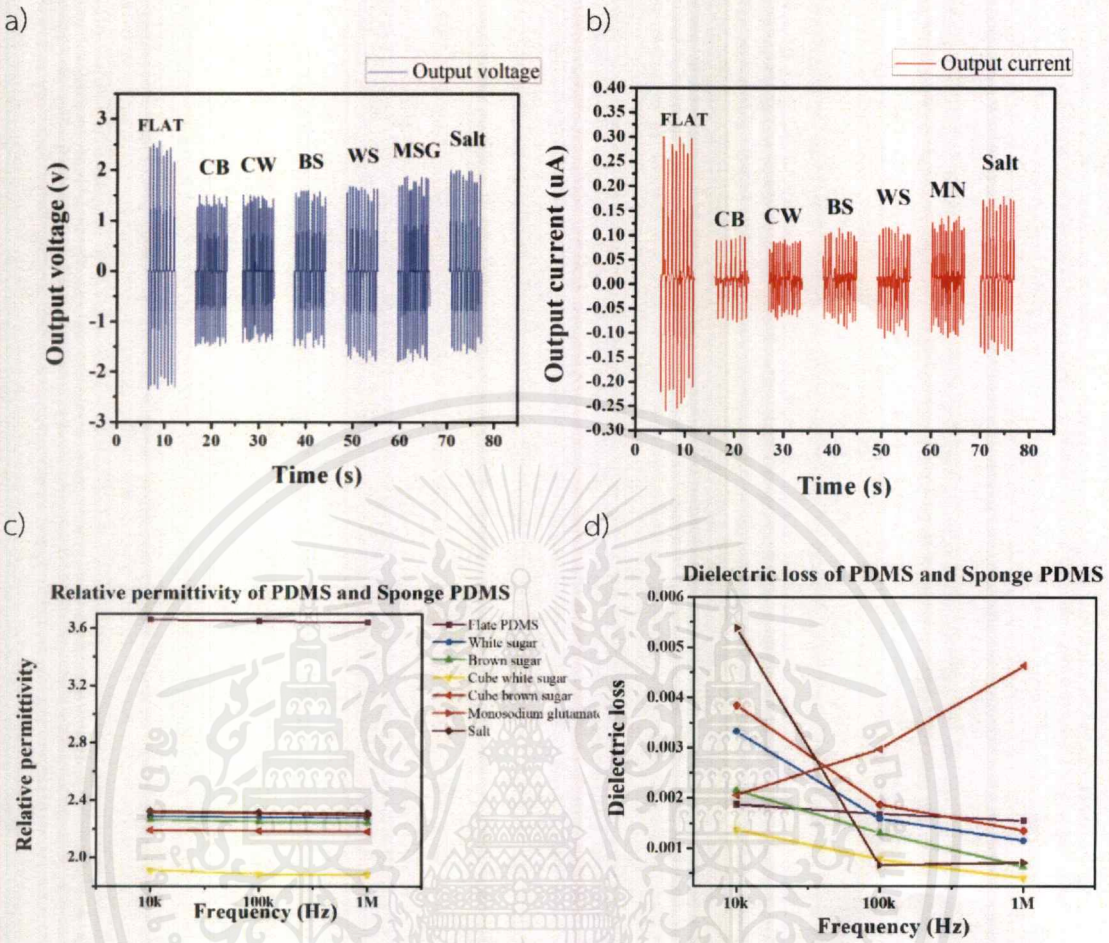

Figure 4.7 Electrical output performance of the Flat and Sponge PDMS. a) V_{oc} and b) I_{sc} and Dielectric property measurement, c) Dielectric constant and d) Dielectric loss in a frequency at 10 kHz, 100 kHz and 1 MHz.

We investigated the electrical characterization of the fabricated TENG, the V_{oc} and I_{sc} were measured. For a fair comparison, the volume of samples,the applied force and frequency are identical.

Working mechanism of TENG in the generate electrical power, as presents in APPENDIX B Figure S4.1. And the recorded values are shown in Figure 4.7 a) and b), the PDMS flat provides the greater output performance than all PDMS sponges with V_{oc} and I_{ac} values at 2.2 V and 2.2 μA. Then, the Salt – PDMS sponge shows the highest output V_{oc} (1.91 V) and I_{ac} (0.14 μA) as compared to the other PDMS sponges that were fabricated by different template.

4.1.2.2 Dielectric measurement

In principle, the output performance of TENGs depends on triboelectric charges density (**σ**). At the open-circuit (OC) condition, there is no charge transfer, which means

that $\Delta\sigma$ is 0. Therefore, the open-circuit voltage is correlated with the dielectric property of sample.

Dielectric property was performed in dielectric measurement step in this work for Flat and Sponges PDMS in a frequency at 10 kHz, 100 kHz and 1 MHz (value in APPENDIX A Table. A4.4). In addition, Dielectric loss values were collected together with Dielectric constant measurement, as shows comparisons in Figure 4.7 c) and d), the Dielectric constant of the Flat and Sponge PDMS dropped from 3.6 to 1.5 at 1M Hz with the increase in %Porosity from 0% to 75%. The values of the pore characterization as shows in APPENDIX A Table A4.3, the pores in the sponge PDMS can be regarded just as the filling particles with the permittivity of air ε_r = 1 (lower than that of PDMS). The lower dielectric particles filling in the PDMS result in reduction in effective permittivity [41, 44].

4.2 The fabricated composite PDMS sponge

4.2.1 The composite g-C_3N_4/PDMS sponge

4.2.1.1 Characterizations

4.2.1.1.1 Scanning electron microscope (SEM) measurement

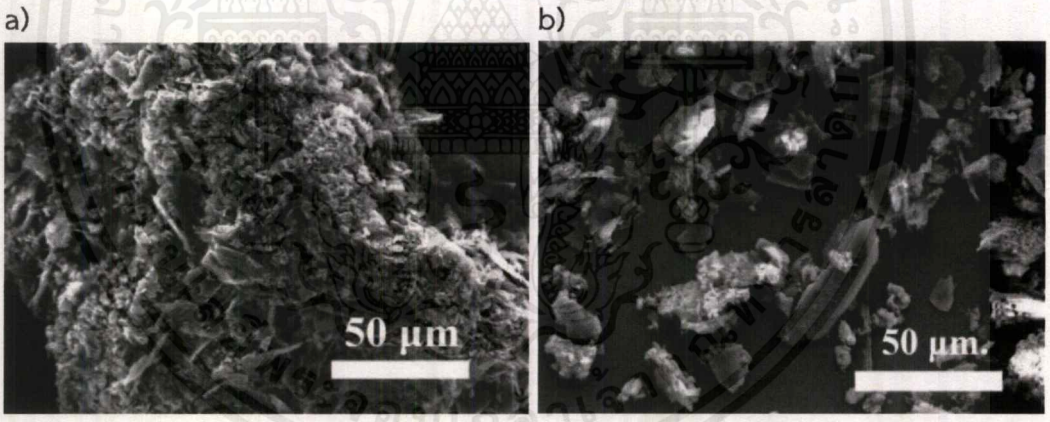

Figure 4.8 SEM images show a) the morphologies and b) the distribution of g-C_3N_4.

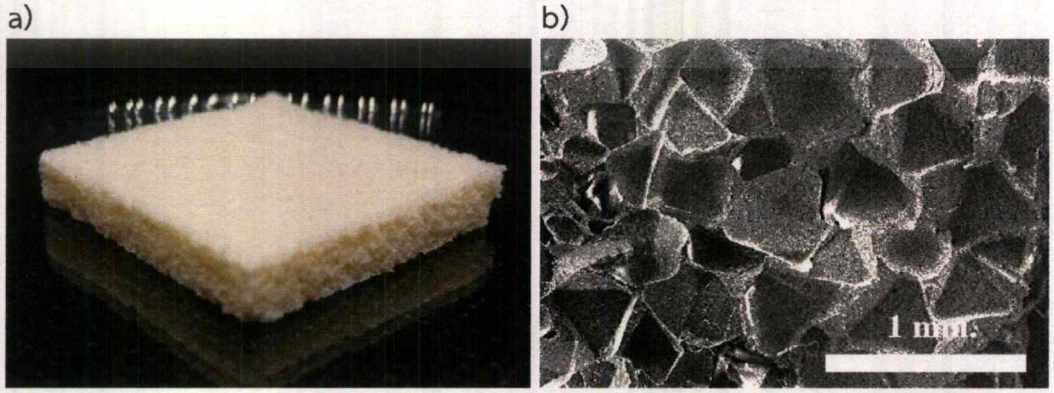

Figure 4.9 a) Photograph and b) SEM image of the cross – sectional area of the of the fabricated g-C_3N_4/PDMS sponge.

In Figure 4.8 a) and b) show the morphologies of g-C_3N_4 that have the size average around 24 micrometers. After leaching process, obtained composite PDMS sponge is presented by Figure 4.9 a) The shape and size of the porous inside it shows in the Figure 4.9 b), its morphologies were not different from the pure PDMS sponge that obtained by using Salt template.

4.2.1.1.2 Fourier transform infrared spectroscopy (FT-IR) measurement.

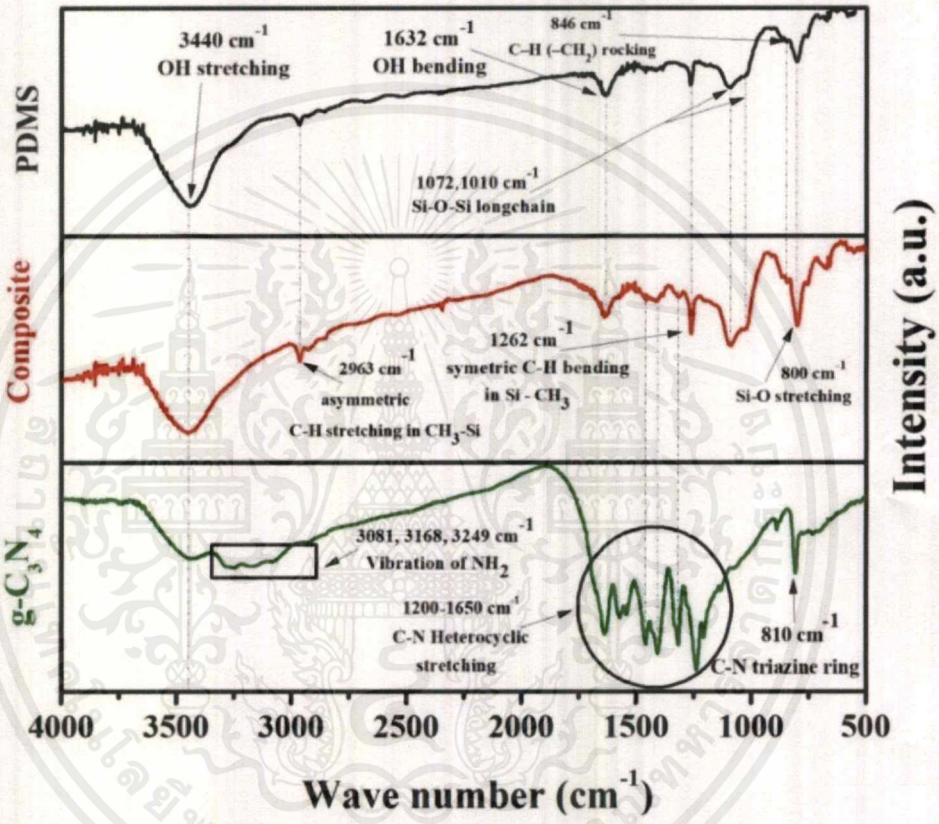

Figure 4.10 Infrared spectra of PDMS sponge, g-C_3N_4/PDMS composite sponge by templating and g-C_3N_4 powder were recorded using a FT-IR (FTIRSPECTRUM GX) at spectral range 400 – 4000 cm^{-1}.

The g-C_3N_4/PDMS composite sponge show the Infrared spectra in Figure 4.10, the characteristic peak of g-C_3N_4 is related bonding of C-N heterocyclic stretching around at 1200 – 1650 cm^{-1} that can be found in the sponge composite and found peak around at 810 cm^{-1} is related to triazine ring in the structure, board peak around at 3081, 3168, and 3294 is corresponding to the vibration of NH_2 group [45] and this spectra not found the vibration of bonded atom between PDMS (matrix phase) and g-C_3N_4 (dispersed phase).

4.2.1.1.3 X-Ray diffraction (XRD).

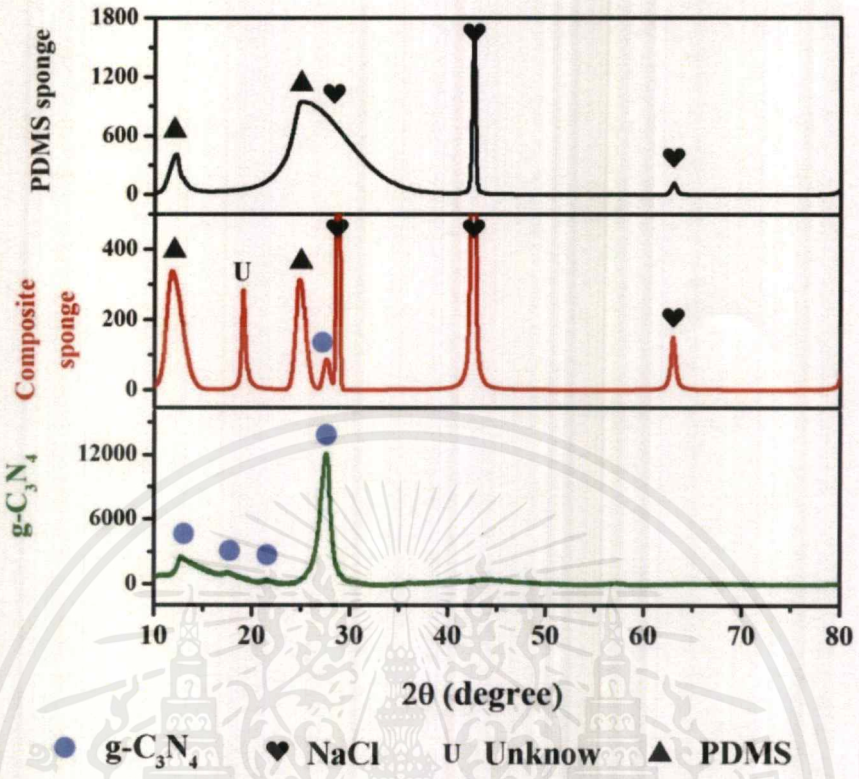

Figure 4.11 The XRD pattern of PDMS sponge, g-C_3N_4 - PDMS composite sponge by templating technique and g-C_3N_4 powder were recorded by X-ray diffraction (XRD, (D8 Advance, Bruker AXS) at the rang 10 – 80° .

The XRD pattern in Figure 4.11 shows the investigation of g-C_3N_4/PDMS composite sponge by templating technique, which fabricated from PDMS silicone polymer mix g-C_3N_4 powder and used salt as a template, the pattern of g-C_3N_4 /PDMS composite sponge as show the PDMS pattern at around 2Θ = 11.9 and 24.8 degree, the formation of peak at 11.9 to confirming the presence of ordered regions of PDMS. A second and broader peak is also observed at 2Θ at around 21.1 in the irradiated PDMS. This amorphous peak is typical of amorphous silica and is associated to the distance between Si atoms in the PDMS backbone (Si–O–Si) [46]. After that we found the peak of NaCl phase, at around 2Θ = 28.7, 42.6, 62.9 degree that close to the pattern of NaCl JCPDS card number 83-1728 and the peak of unknown phase show at around 19.0 degree that we assumed it is the plate of sample in instrument. The important pattern of Graphitic carbon nitride (dispersed phase) show important peak at around 2Θ = 27.6 degree and small peak around at 12.7, 17.5 and 21.8 degree [47] but in the g-C_3N_4/PDMS sponge can be found the only peak at 27.6 demonstrate that it has the graphitic carbon nitride in the composite structure and not found the new

bonding between PDMS and g-C_3N_4 phase, form this we are assumed that the sponge form mix polymer is be a composite.

4.2.1.1.4 Contact angle measurement

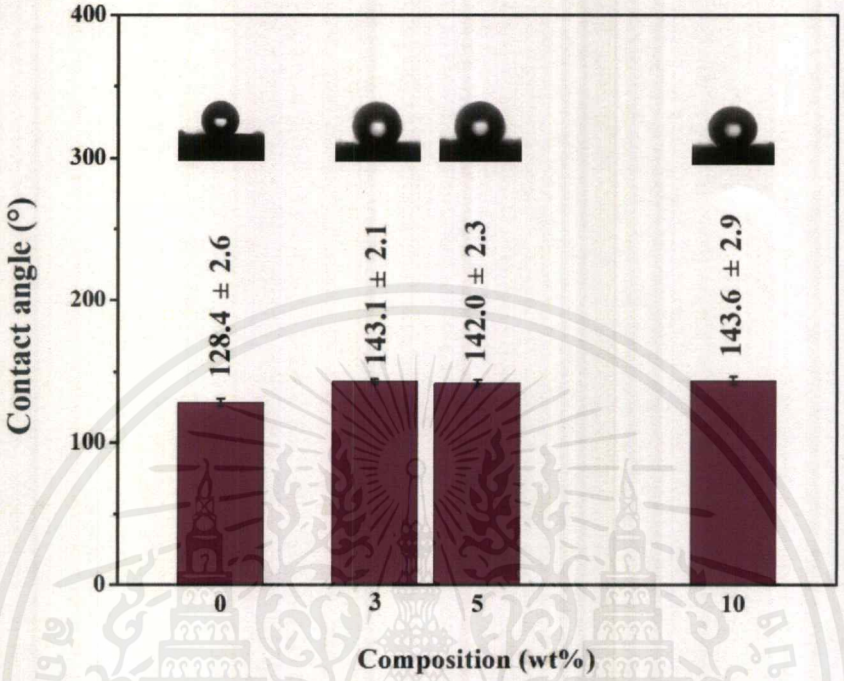

Figure 4.12 Contact angle on the g-C_4N_3/PDMS sponge surfaces with optical images of water droplets.

The effect of the various g-C_4N_3 concentrations on the surface wettability of composite PDMS sponges was investigated, resulting as shows in Figure 4.12, the contact angle of the g-C_4N_3/PDMS sponges are higher than the Salt –PDMS sponge because the g-C_4N_3 material more exposes on the surface of the composite. Moreover, the contact angle of the g-C_4N_3/PDMS sponges from various concentrations is not different significantly.

4.2.1.2 Mechanical measurement

4.2.1.2.1 Manual Testing

Table 4.2 Photograph of the composite g-C_3N_4/PDMS sponge with various g-C_3N_4 concentrations and Manual testing

g-C_4N_3 (wt%)	Composite PDMS sponge	Manual testing	
		Bending	Twisting
1	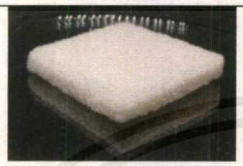	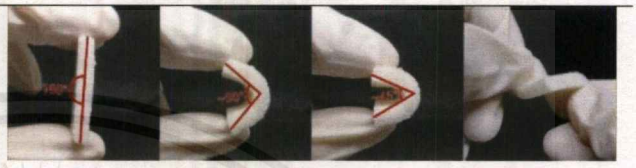	
3			
5			
10			

The fabricated g-C_3N_4/PDMS sponges and its response under applying force in manual testing, as shows in Table 4.2, are not different from the Salt - PDMS sponge. However, when the applied force was released from these samples, it didn't recover to original shape immediately. We are assumed that the g-C_3N_4 particles obstructed the polymerization of PDMS.

4.2.1.2.2 Compression testing

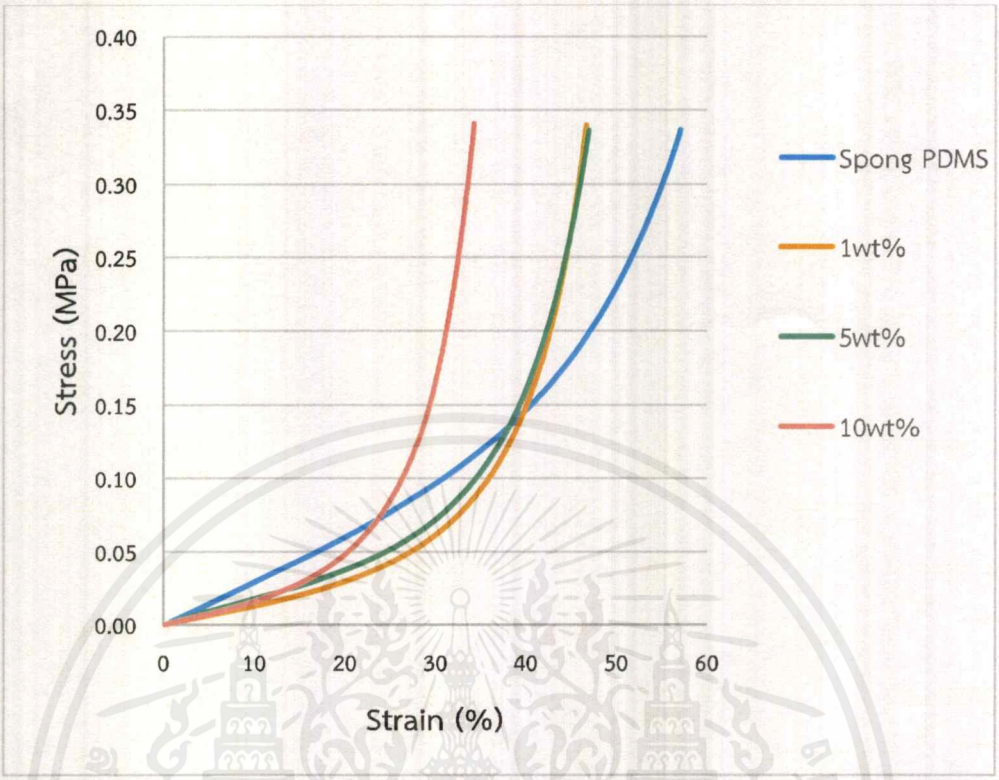

Figure 4.13 Stress – strain curves of the Flat and Sponges PDMS under constant-force compression at 300 N.

Compression testing was investigated to study mechanical properties of the fabricated composite PDMS sponges. The stress – strain curves of the four samples are presented in Figure 4.13, compared to the PDMS flat, the three curves of the composite sponges have more shift. These implied that the composite PDMS sponges consist of g-C_3N_4 particles as a filler material, then increase the g-C_3N_4 concentration, the hardness of composite PDMS sponges can be increased. As confirmed by resulting of elastic modulus, as shows in APPENDIX A Table A4.2, the elastic modulus of the g-C_3N_4/PDMS sponges increase from 0.49 MPa to 0.68 MPa with increase in the g-C_3N_4 concentration from 1 to 10 %wt.

4.2.1.3 Electrical measurement

4.2.1.3.1 The output voltage and current performance of TENG

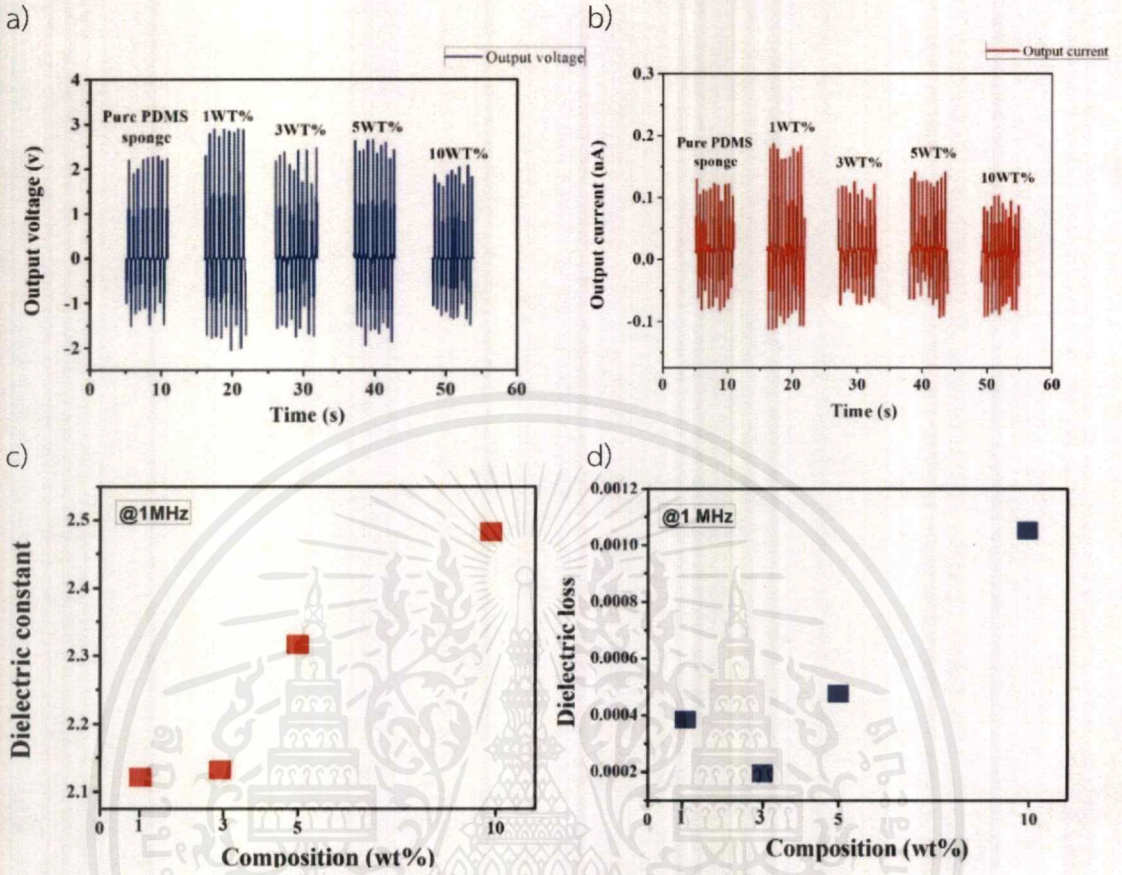

Figure 4.14 Electrical output performance and Dielectric properties of the g-C_3N_4/PDMS sponges with various g-C_3N_4 concentrations. a) V_{oc}, b) I_{sc}, c) Dielectric constant and d) Dielectric loss in a frequency at 1 MHz.

The effect of g-C_3N_4 concentration on output voltage and current was investigated. The output performance of the various g-C_3N_4/PDMS sponges are not a trend, as shows in Figures 4.14 a) and b). With the g-C_3N_4 concentration is 1 %wt, the output V_{oc} and I_{sc} presents at 1.90 V and 0.17 μA that are more than the Salt-PDMS sponge. However, when the g-C_3N_4 content increase more 3 %wt, the output performance slightly decreases. These results are not related to dielectric measurement, as shows in Figures 4.14 c), We suspect that in the electrical generating process, when the applied force was released from g-C_3N_4/PDMS sponge. it didn't immediately recover to original shape. This problem may be effect on the electrical generating of TENG.

4.2.1.3.2 Dielectric measurement

As presents in Figures 4.14 c) and d), when the g-C_3N_4 content increases, the Dielectric constant dramatically increases and reach its maximum value at 2.49 when the content is 10 %wt.

4.2.3 The Fabrication Graphite fluoride/PDMS sponge

4.2.3.1 Characterization

4.2.3.1.1 Scanning electron microscope (SEM).

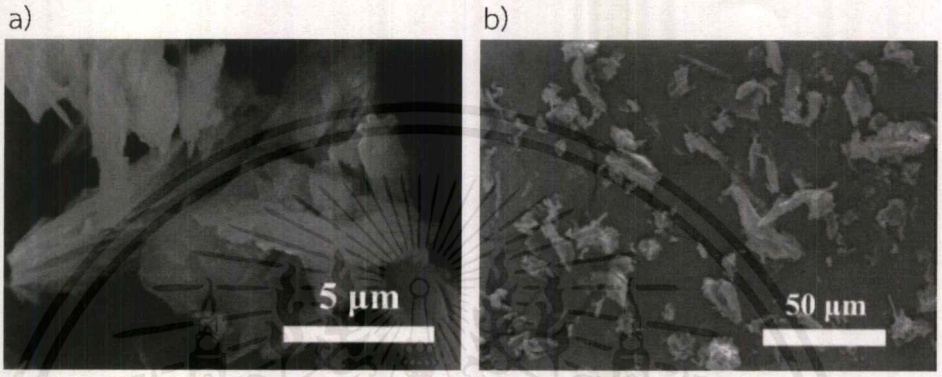

Figure 4.15 SEM images show a) the morphologies and b) the distribution of Graphite fluoride.

The photograph in Figure 4.15 that shows the morphologies of carbon allotropes dispersed phase on the different magnificent. Figures 4.16 a) and b) show the morphologies of Graphite fluoride stacks and 2D shape for each layer have size average around at 7 micrometers. After dispersed the carbon allotrope in the PDMS matrix phase until leaching the salt template, the composite PDMS sponge that has the shape and size of the porous inside it shows in the Figure 4.16 below.

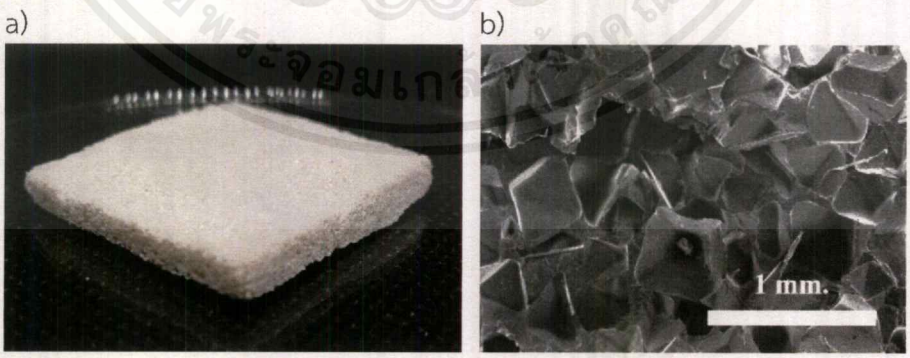

Figure 4.16 a) Photograph and b) SEM image of the cross – sectional area of the of the fabricated Graphite fluoride/PDMS sponge.

4.2.3.1.2 Fourier transform infrared spectroscopy (FTIR).

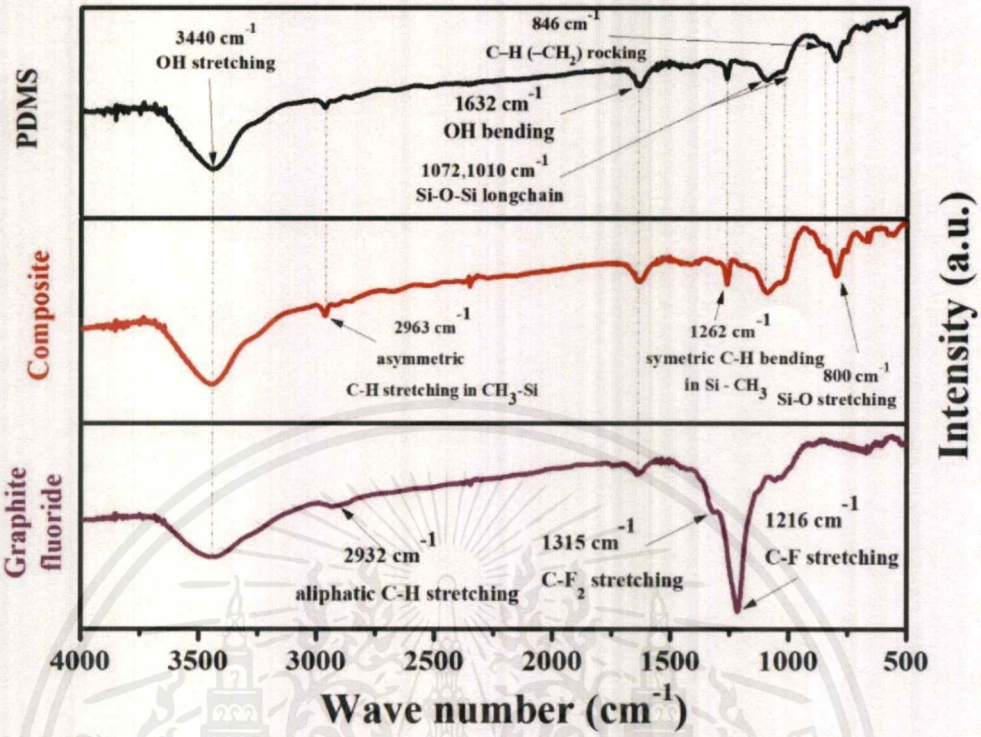

Figure 4.17 Infrared spectra of PDMS sponge, Graphite fluoride - PDMS composite sponge by templating technique and Graphite fluoride powder were recorded using a FT-IR (FTIRSPECTRUM GX) at spectral range 400 – 4000 cm^{-1}.

The infrared spectra in Figure 4.17. as shows the characteristic peak of Graphite fluoride around at 1216 cm^{-1} is corresponding to the stretching of C-F bond and the shoulder around at 1315 cm^{-1} is relate C-F_2 stretching [48]. According to the infrared spectra of composite sponge in Figure. 4.17 not found the characteristic peak of Graphite fluoride in Graphite fluoride/PDMS sponge and not found the vibration of bonded atom between PDMS (matrix phase) and Graphite fluoride (dispersed phase) that notice it is a completely composite.

4.2.3.1.3 X-Ray diffraction (XRD).

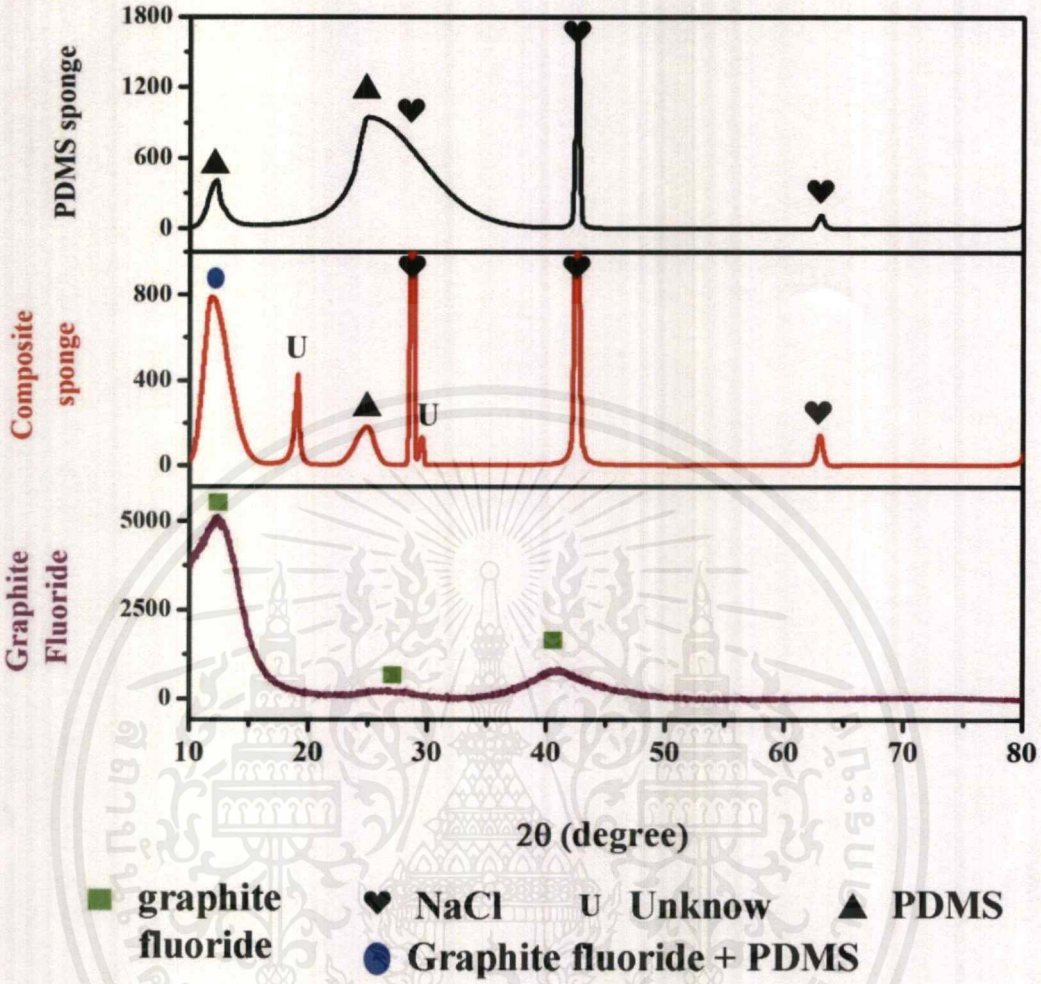

Figure 4.18 The XRD pattern of The Salt – PDMS sponge, Graphite fluoride/PDMS sponge by templating and Graphite fluoride powder were recorded by X-ray diffraction (XRD, (D8 Advance, Bruker AXS) at the rang 10 – 80°.

The XRD pattern in figure 4.18 show the pattern of Graphite fluoride - PDMS composite sponge by templating technique which fabricated from PDMS silicone polymer composite with graphite fluoride powder and use salt in templating process, the pattern of graphite fluoride - PDMS composite sponge as show the pattern of PDMS at around 2Θ = 11.9 and 24.8 degree that formation of peak at 11.9 caused by a ribbon like conformation of PDMS with folded chains. It confirmed the presence of ordered regions of PDMS. This shows that in these hybrid samples the polymer prefers to coil itself rather than being mingled with the inorganic matrix. A second and broader peak is also observed at 2Θ at around 21.1 in the irradiated PDMS. This peak reflects short range order, it is typical of amorphous silica and is associated to the distance between

Si atoms in the PDMS backbone (Si–O–Si) [46] after that we still found NaCl phase at around 2θ = 28.7, 42.6, 62.9 degree that close to the pattern of NaCl JCPDS card number 83-1728 but not found the pattern of Graphite fluoride (dispersed phase), which have important peak at around 2θ = 12.3 degree and board peak around at 26.1, 40.8 degree [48] but in composite (Graphite fluoride - PDMS) sponge found the peak around at 12.3 combined with peak around at 11.9 degree this reason make the peak are high intensity and we found the unknown phase at around 19.0 and 29.5 degree that we assumed it is the plate of sample in instrument. summarize, form this information that demonstrate that we cannot leaching salt template from the PDMS sponge and Graphite fluoride - PDMS composite sponge completely.

4.2.3.1.4 Contact angle measurement

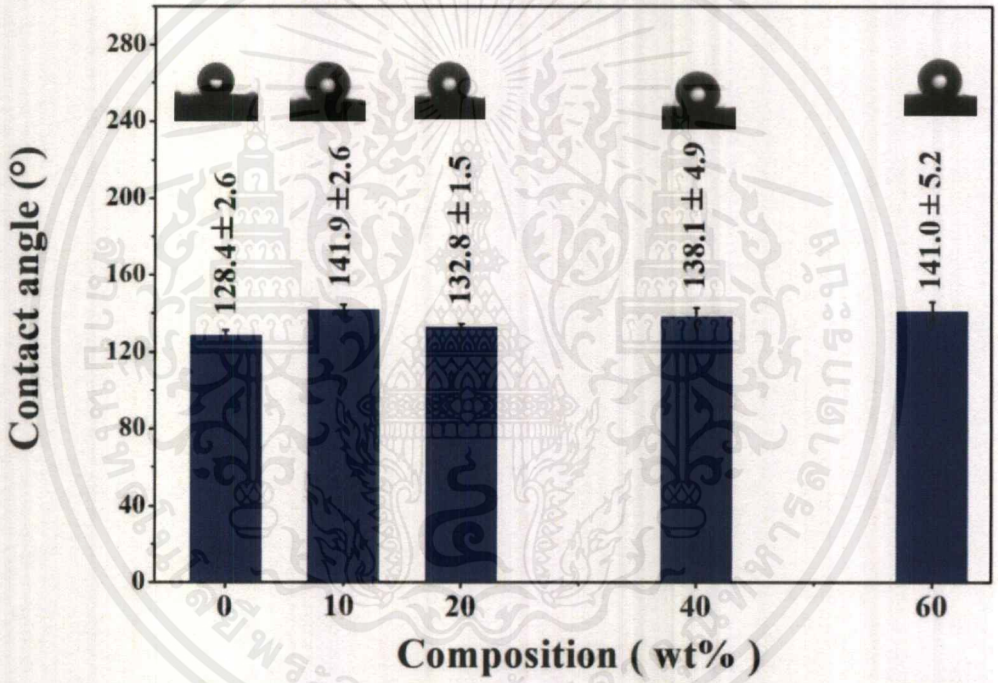

Figure 4.19 Contact angle of water droplet on the Graphite fluoride/PDMS sponge surfaces with various Graphite fluoride concentrations

The effect of the various Graphite fluoride concentrations on the surface wettability of composites PDMS sponges was investigated by contact angle measurement, resulting as shows in Figure 4.19 the contact angle of water droplet in each the Graphite fluoride/PDMS sponge surface were not different significantly. In addition, the composite PDMS sponges remain in ultra-hydrophobic character as the Salt-PDMS sponge.

4.2.3.2 Mechanical measurement

4.2.3.2.1 Manual testing

Table 4.3 Photograph of the Graphite fluoride/PDMS sponges with various Graphite fluoride concentrations and Manual testing

Graphite fluoride (wt%)	Composite PDMS sponge	Manual testing	
		Bending	Twisting
10	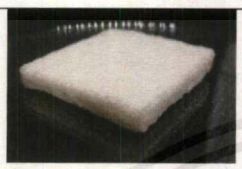	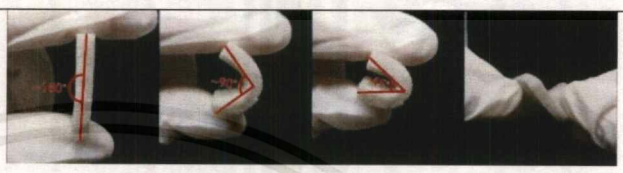	
20	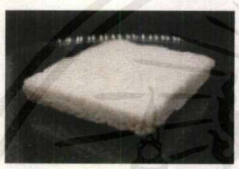		
40			
60			

The fabricated Graphite fluoride/PDMS sponges and its response under applying force in manual testing, as shows in Table 4.3, are not different from the Salt - PDMS sponge. Noteworthy, the Graphite fluoride/PDMD sponges have hardened markedly increased concentration of Graphite fluoride.

4.2.3.2.2 Compression testing

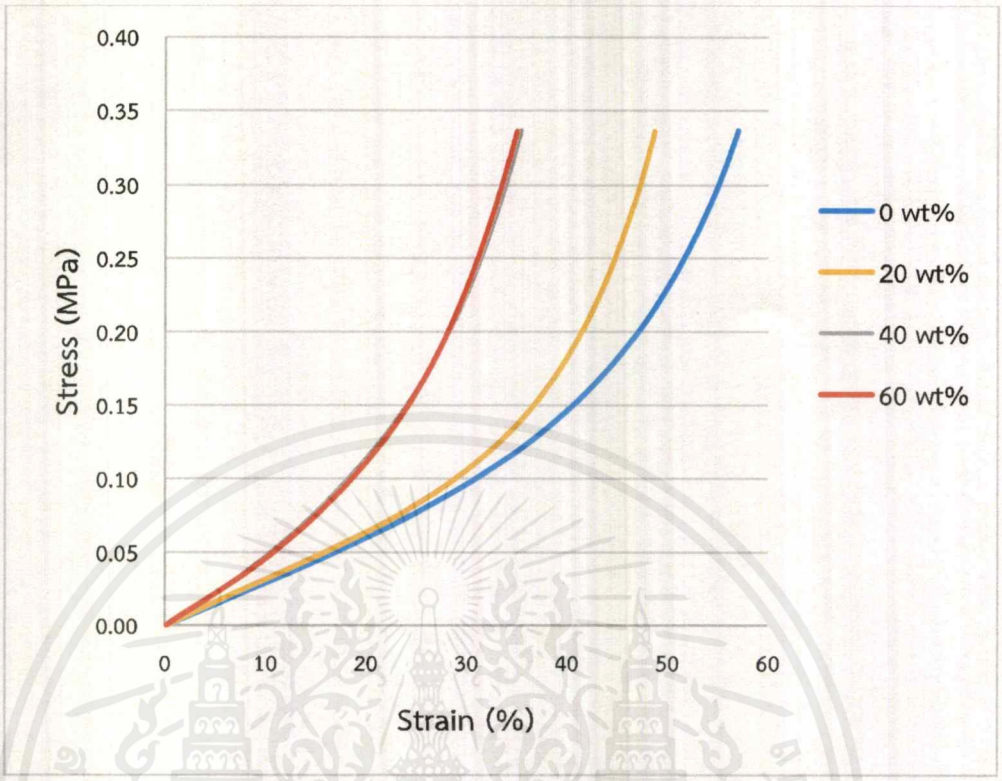

Figure 4.20 Stress – strain curves of the Graphite fluoride/PDMS sponges with various Graphite fluoride contents under constant-force compression at 300 N.

Compression testing was investigated to study mechanical properties of the fabricated composite PDMS sponges. The stress – strain curves of the four samples are presented in Figure 4.20, compared to the PDMS flat, the three curves of the composite sponges have more shift. These implied that the composite PDMS sponges consist of Graphite fluoride particles as a filler material, then increase the Graphite fluoride concentration, the hardness of composite PDMS sponges can be increased. As confirmed by resulting of elastic modulus, as shows in APPENDIX A Table 4.2, the elastic modulus of the Graphite fluoride/PDMS sponges increase from 0.56 MPa to 0.86 MPa with increase in the Graphite fluoride concentration from 20 to 60 %wt.

4.2.2.3 Electrical measurement

4.2.2.3.1 The output voltage and current performance of TENG

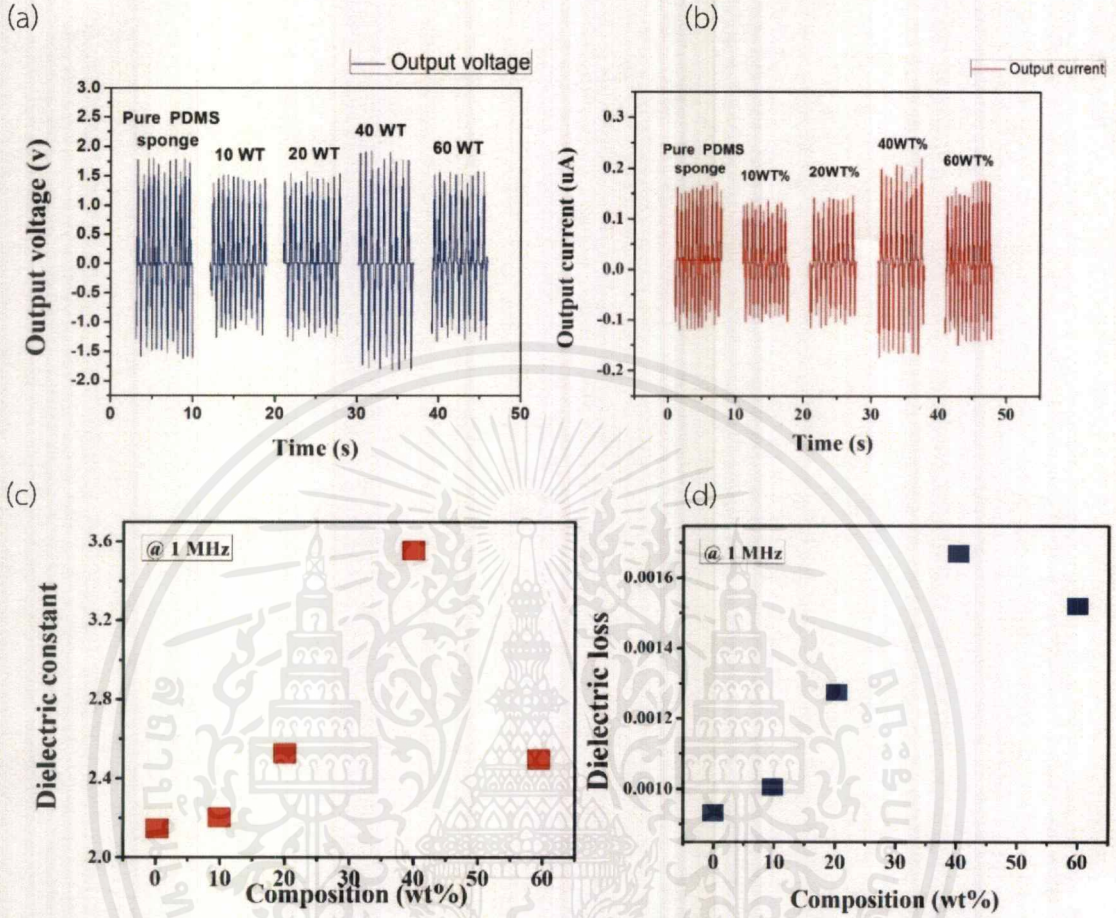

Figure 4.21 Electrical output performance and Dielectric properties of the Graphite fluoride/PDMS sponges with various Graphite fluoride concentrations. a) V_{oc}, b) I_{sc}, c) Dielectric constant and d) Dielectric loss under certain frequency measurement at 1 MHz

First, the effect of Graphite fluoride concentration on its voltage and current outputs was investigated. The output performance of the various Graphite fluoride/PDMS sponges exhibit a notably similar trend, as shows in Figure 4.21 b). As the Graphite fluoride concentration increases, the output voltage and current reach their maximum values of 1.82 V and 0.20 μA, respectively, with the 40 %wt Graphite fluoride concentration. However, the output performance decreases with the increase of Graphite fluoride concentration at 60 %wt. These results according to the resulting of the dielectric measurement, as shows in Figure 4.21 b), which indicated that the Dielectric constant increases with Graphite fluoride content up to 40 wt% and drop at 60 %wt.

4.2.2.3.2 Dielectric measurement

As presents in Figure 4.21, the Graphite fluoride concentration profoundly effect on the dielectric properties. When the Graphite fluoride content increases, the Dielectric constant dramatically increases and reaches its maximum value at 3.55 when the content is 40 %wt.

CHAPTER 5
CONCLUSIONS AND SUGGESTIONS

5.1 Conclusions

5.1.1 The fabrication of the PDMS sponge by templating

In this report, we have fabricated PDMS sponge by different type of particles as a template. For this method, we succeeded in fabricating PDMS sponge by templating. Its characteristics, such as porosity and distribution can be controlled by template selection. For contact angle measurement, the PDMS sponges show higher value than the PDMS flat and among of PDMS sponges, the salt – PDMS sponge shows the highest hydrophobicity at 128°. In addition, the PDMS sponges exhibit higher mechanical softness than the PDMS flat, as evidenced by the compliance value at 185.04, which is 7 – time higher than the flat PDMS. Resulting in output performance and dielectric measurement, The TENG of the salt – PDMD sponge can generate output voltage and current up to 1.91 V and 0.14 μA, respectively, and show the highest dielectric constant at 2.31, compared with the other PDMS sponge.

5.1.2.1 Composite g-C_3N_4/PDMS sponge

The composite g-C_3N_4/PDMS sponges show the morphologies and the response under applying of manual testing are not different from the salt – PDMS sponge. However, it does not recover to original shape immediately when the applied force was released. For mechanical property, the elastic modulus of the g-C_3N_4/PDMS sponges increase from 0.49 MPa to 0.68 MPa with increase in the g-C_3N_4 concentration from 1 to 10 %wt. Resulting in output performance, the various g-C_3N_4 concentration on composite PDMS sponges are not a trend in the change of output voltage and current. Nevertheless, when the g-C_3N_4 content increase, the dielectric constant also increases and reaches its maximum value at 2.49 when the content is 10 %wt.

5.1.2.2 Composite Graphite fluoride/PDMS sponge

The composite Graphite fluoride/PDMS sponges show the morphologies and the response under applying of manual testing are not different from the salt – PDMS sponge. However, when the Graphite fluoride content increase, the composite/PDMS sponges are hardened markedly. As evidenced by resulting of compression measurement, the elastic modulus of the Graphite fluoride/PDMS sponges increase from 0.56 MPa to 0.86 MPa with increase in the Graphite fluoride concentration from 20 to 60 %wt. Resulting in output performance, as the concentration increase, the output voltage and current reach its maximum values at 1.82 V and 0.20 μA,

respectively, with the 40 wt% of Graphite fluoride. As the same concentration, the composite PDMS sponge also shows its dielectric constant at 3.55.

5.2 Suggestions

5.2.1 Increase the amount of time in template leaching.

5.2.2 Increase the applied force that was used to press TENG.

5.2.3 Fabrication PDMS sponge in another way such as use water for microwave radiation fabrication.

REFFERENCES

[1] Song, Xiaoxu & Hu, Shanying & Chen, Dingjiang & Zhu, Bing. (2017). "Estimation of Waste Battery Generation and Analysis of the Waste Battery Recycling System in China." **Journal of industrial ecology**. Vol.21 : 57-69.

[2] Ling Bing Kong, Tao Li, Huey Hoon Hng, Freddy Boey, Tianshu Zhang, and Sean Li. 2015. **Waste Energy Harvesting: Mechanical and Thermal Energies.** Germany : WILEY-VCH Verlag GmbH & Co. KGaA, Weinheim.

[3] Feng-Ru Fana, Zhong-Qun Tian , Zhong Lin Wang. (2012). "Flexible Triboelectric Generator" **Nano energy**. Vol.1(No. 2) : 328-334.

[4] Lee,Jae Won and Ye,Byeong Uk and Baik,Jeong Min. (2017). "Research Update: Recent progress in the development of effective dielectrics for high-output triboelectric nanogenerator." **APL materials**. Vol.5(7) : 073802.

[5] Guang Zhu, Bai Peng, Jun Chen, Qingshen Jing, Zhong Lin Wang. (2015). "Triboelectric nanogenerators as a new energy technology: From fundamentals, devices, to applications." **Nano energy**. Vol.14 : 126-138.

[6] Ma, Mingyuan and Kang, Zhuo and Liao, Qingliang and Zhang, Qian and Gao, Fangfang and Zhao, Xuan and Zhang, Zheng and Zhang, Yue. (2018) . "Development, applications, and future directions of triboelectric nanogenerators." **Nano research**. Vol.11(6) : 2951-2969.

[7] Duan, Shasha and Yang, Ke and Wang, Zhihui and Chen, Mengting and Zhang, Ling and Zhang, Hongbo and Li, Chunzhong. (2016). "Fabrication of Highly Stretchable Conductors Based on 3D Printed Porous Poly(dimethylsiloxane) and Conductive Carbon Nanotubes/ Graphene Network." **ACS applied materials & interfaces**. Vol.8(3) : 2187-2192.

[8] Zhao, Jian and Luo, Gaoxing and Wu, Jun and Xia, Hesheng. (2013) . "Preparation of Microporous Silicone Rubber Membrane with Tunable Pore Size via Solvent Evaporation- Induced Phase Separation." **American Chemical Society**. Vol.5(6) : 2040-2046.

[9] Choi, Sung-Jin and Kwon, Tae-Hong and Im, Hwon and Moon, Dong-Il and Baek, David J. And Seol, Myeong-Lok and Duarte, Juan P. and Choi, Yang-Kyu. (2011). "A Polydimethylsiloxane (PDMS) Sponge for the Selective Absorption of Oil from Water." **ACS applied materials & interfaces**. Vol.3 (12) : 4552-4556.

[10] Kim, D, Park, Sang-Jae, Jeon, Seung-Bae, Seol, Myeong-Lok, Choi, Yang-Kyu (2016). "A Triboelectric Sponge Fabricated from a Cube Sugar Template by 3D Soft Lithography for Superhydrophobicity and Elasticity." **Adv. Electron. Mater.** Vol.2 : 1500331.

[11] Zhang Aijuan, Chen Mingjie, Guo Huizhang, Hua, Bai and li, Lei (2013). "Poly(dimethylsiloxane) Oil Absorbent with a Three-Dimensionally Interconnected Porous Structure and Swellable Skeleton." **ACS applied materials & interfaces.** Vol.5.

[12] Zhao Xia, Li Lingxiao, Li Bucheng, Zhang Junping and Wang Aiqin. (2014). "Durable superhydrophobic/superoleophilic PDMS sponges and their applications in selective oil absorption and in plugging oil leakages" **J. Mater. Chemistry A.** Vol.2(43) : 18281-18287.

[13] Jang Shin and Oh Je Hoon. (2018). "Rapid Fabrication of Microporous BaTiO3/PDMS Nanocomposites for Triboelectric Nanogenerators through One-step Microwave Irradiation." **Scientific reports.** Vol.8(1). : 14287.

[14] Zhu Yanbo,Yang Bin, Liu Jingquan, Wang, Xingzhao, Wang, Luxian, Chen, Xiang, Yang, Chunsheng. (2016). "A flexible and biocompatible triboelectric nanogenerator with tunable internal resistance for powering wearable devices." **Scientific reports.** Vol.6 : 22233.

[15] Kim Jeong Hun, Hwang Ji-Young, Hwang Ha Ryeon, Kim Han Seop, Lee Joong Hoon, Seo Jae-Won, Shin Ueon Sang and Lee Sang-Hoon. (2018). "Simple and cost- effective method of highly conductive and elastic carbon nanotube/ polydimethylsiloxane composite for wearable electronics." **Scientific reports.** Vol.8(1) : 1375.

[16] Fan, Youjun and Song Meng, Xian and Yang Li, Hua and Kuang, Shuang and Zhang, Lei and Wu, Ying and Wang, Zhong and Zhu, Guang. (2016). "Stretchable Porous Carbon Nanotube-Elastomer Hybrid Nanocomposite for Harvesting Mechanical Energy." **Advanced materials.** Vol.29.

[17] Choi, Young-Soo and Gwak, Min-Joo and Lee, Dong-Weon. (2016). "Polymeric cantilever integrated with PDMS/graphene composite strain sensor." **Review of Scientific Instruments.** Vol.87.

[18] Liang, Suqing and Li, Yaoyao and Chen, Yuzhen and Yang, Jinbin and Zhu, Taipeng and Zhu, Deyong and He, Chuanxin and Liu, Yizhen and Handschuh-Wang, Stephan and Zhou, Xuechang. (2017). "Liquid metal sponges for mechanically durable, all-soft, electrical conductors." **J. Mater. Chem. C.** Vol.5(7). : 1586-1590.

[19] Wang, Jie and Zhou, Linglin and Zhang, Chunlei and Wang, Zhong. 2019. **Small-Scale Energy Harvesting from Environment by Triboelectric Nanogenerators.** [Online]. Available : https://www.intechopen.com/online-first/small-scale-energy-harvesting-from-environment-by-triboelectric-nanogenerators

[20] Chi Zhang, Zhong Lin Wang. 2017. **Triboelectric Nanogenerators.** Singapore : Springer.

[21] Lin, Zhiming and Chen, Jun and Yang, Jin, (2016). "Recent Progress in Triboelectric Nanogenerators as a Renewable and Sustainable Power Source." **Journal of nanomaterials.** Vol.2016 : 1-24.

[22] Joo Kim, Yeon and Lee, Jaejun and Park, Sangwon and Park, Chanho and Park, Cheolmin and Choi, Heon-Jin. (2014). "Effect of the relative permittivity of oxides on the performance of triboelectric nanogenerators." **RSC Adv.** Vol.7 : 49368-49373.

[23] A Nafari and H A Sodano. (2017). "Surface morphology effects in a vibration based triboelectric energy harvester." **Smart materials and structures.** Vol.27(1) : 015029

[24] Zhu, Deyong and Handschuh-Wang, Stephan and Zhou, Xuechang. (2017). "Recent progress in fabrication and application of polydimethylsiloxane sponges." **J. Mater. Chem. A.** Vol.5(32). : 16467-16497.

[25] Jang Shin and Oh Je Hoon. (2018). "Rapid Fabrication of Microporous BaTiO3/PDMS Nanocomposites for Triboelectric Nanogenerators through One-step Microwave Irradiation." **Scientific reports.** Vol.8(1). : 14287.

[26] Edson Cocchieri Botelhoa, Rogério Almeida Silvac, Luiz Cláudio Pardinia , Mirabel Cerqueira Rezendea. "A review on the development and properties of continuous fiber/epoxy/aluminum hybrid composites for aircraft structures." **Materials research.** Vol.9 : 247 – 256.

[27] Mohammed Khalifa, Arunjunairaj Mahendran, S. Anandhan. (2019). "Synergism of graphitic- carbon nitride and electrospinning on the physico- chemical characteristics and piezoelectric properties of flexible poly(vinylidene fluoride) based nanogenerator." **Journal of polymer research.** Vol.26(3) : 73.

[28] Kihong Kim, Giyoung Song, Cheolmin Park, and Kwang-Seok Yun. (2017) . "Multifunctional Woven Structure Operating as Triboelectric Energy Harvester, Capacitive Tactile Sensor Array, and Piezoresistive Strain Sensor Array." **Sensors.** vol. 17(11) : 2582.

[29] Wang, Zepu and Nelson, J. Keith and Hillborg, Henrik and Zhao, Su and Schadler, Linda S. (2012). "Graphene Oxide Filled Nanocomposite with Novel Electrical and Dielectric Properties." **Advanced materials.** Vol.24(23) : 3134-3137.

[30] Harnchana Viyada, Ngoc Huynh Van, He Wen, Rasheed Aamir, Park Hyunje, Amornkitbamrung Vittaya, Kang Dae Joon. (2018), "Enhanced Power Output of a Triboelectric Nanogenerator Using Poly(Dimethylsiloxane) Modified with Graphene Oxide and Sodium Dodecyl Sulfate." **ACS applied materials & interfaces**, Vol. 10(30) : 25263-25272.

[31] Yanbo Zhu, Bin Yang, Jingquan Liu, Xingzhao Wang, Luxian Wang, Xiang Chen, and Chunsheng Yang. (2016) . "A flexible and biocompatible triboelectric nanogenerator with tunable internal resistance for powering wearable devices." **Sci report.** Vol.6 : 22233.

[32] Fan, Youjun and Song Meng, Xian and Yang Li, Hua and Kuang, Shuang and Zhang, Lei and Wu, Ying and Wang, Zhong and Zhu, Guang. (2016) . "Stretchable Porous Carbon Nanotube-Elastomer Hybrid Nanocomposite for Harvesting Mechanical Energy." **Advanced materials.** Vol.29

[33] Duan Shasha, Yang Ke, Wang Zhihui, Chen Mengting, Zhang Ling, Zhang Hongbo, Li Chunzhong. (2016). "Fabrication of Highly Stretchable Conductors Based on 3D Printed Porous Poly(dimethylsiloxane) and Conductive Carbon Nanotubes/Graphene Network." **American chemical society.** Vol.8(3) : 2187-2192.

[34] Zhao Jian, Luo Gaoxing, Wu Jun, Xia Hesheng. (2013) "Preparation of Microporous Silicone Rubber Membrane with Tunable Pore Size Via Solvent Evaporation-Induced Phase Separation." **ACS applied materials & interfaces.** Vol. 5(6) : 2040-2046.

[35] Lee, Keun Young and Chun, Jinsung and Lee, Ju-Hyuck and Kim, Kyeong Nam and Kang, Na-Ri and Kim, Ju-Young and Kim, Myung Hwa and Shin, Kyung-Sik and Gupta, Manoj Kumar and Baik, Jeong Min and Kim, Sang-Woo. (2014). "Hydrophobic Sponge Structure-Based Triboelectric Nanogenerator." **Advance materials.** Vol.26 : 5037-5042.

[36] Yu, Cunlong and Yu, Cunming and Cui, Liying and Song, Zhiyang and Zhao, Xinyu and Ma, Ying and Jiang, Lei. (2017). "Facile Preparation of the Porous PDMS Oil-Absorbent for Oil/Water Separation" **Advanced materials interfaces.** Vol.4(3) : 1600862.

[37] Choi Sung-Jin, Kwon Tae-Hong, Im Hwon, Moon Dong-Il, Baek David J., Seol Myeong-Lok, Duarte Juan P. Choi Yang-Kyu. (2011). "A Polydimethylsiloxane (PDMS) Sponge for the Selective Absorption of Oil from Water." **ACS applied materials & interfaces.** Vol.3(12) : 4552-4556.

[38] Zhang, Aijuan and Chen, Mingjie and Guo, Huizhang and Hua, Bai and li, Lei. (2013). Poly(dimethylsiloxane) Oil Absorbent with a Three-Dimensionally Interconnected Porous Structure and Swellable Skeleton. **ACS applied materials & interfaces.** Vol.5.

[39] Johnson, Leah and Gao, Lu and Shields IV, C and Smith, Maggie and Efimenko, Kirill and Cushing, Kevin and Genzer, Jan and P López, Gabriel. (2013). "Elastomeric microparticles for acoustic mediated bioseparations." **Journal of nanobiotechnology.** Vol.11 : 22.

[40] Kim, Daewon and Park, Sang-Jae and Jeon, Seung-Bae and Seol, Myeong-Lok and Choi, Yang-Kyu, (2016). "A Triboelectric Sponge Fabricated from a Cube Sugar Template by 3D Soft Lithography for Superhydrophobicity and Elasticity." **Advanced electronic materials.** Vol.2(4) : 1500331.

[41] Lee, Keun Young and Chun, Jinsung and Lee, Ju-Hyuck and Kim, Kyeong Nam and Kang, Na-Ri and Kim, Ju-Young and Kim, Myung Hwa and Shin, Kyung-Sik and Gupta, Manoj Kumar and Baik, Jeong Min and Kim, Sang-Woo. (2014). "Hydrophobic Sponge Structure-Based Triboelectric Nanogenerator". **Advanced Materials.** Vol.26(29) : 5037-5042.

[42] Maesoon Im, Hown Im, Joo-Hyung Lee, Jun-Bo Yoon and Yang-Kyu Choi. (2010). "A robust superhydrophobic and superoleophobic surface with inverse-trapezoidal microstructures on a large transparent flexible substrate." **Soft matter.** Vol.6(7) : 1401-1404.

[43] ALEX C. M. KUO. 1999. **Polymer Data Handbook**. England : Oxford University Press.

[44] Chen Jie, Guo Hengyu, He Xianming, Liu Guanlin, Xi Yi, Shi Haofei, Hu Chenguo. (2016). "Enhancing Performance of Triboelectric Nanogenerator by Filling High Dielectric Nanoparticles into Sponge PDMS Film." **ACS Applied Materials & Interfaces.** Vol.8(1) : 736-744.

[45] Dai, Hongzhe and Gao, Xuchun and Liu, Enzhou and Yang, YuHao and Hou, WenQian and Kang, LiMin and Fan, Jun and Hu, Xiaoyun. (2013). "Synthesis and characterization of graphitic carbon nitride sub-microspheres using microwave method under mild condition." **Diamond and Related Materials.** Vol.38 : 109-117.

[46] Lancastre, J.J.H. and Fernandes, N and Margaça, Fernanda and Miranda Salvado, I.M. and Ferreira, L and Casimiro, Maria. (2012). "Study of PDMS conformation in PDMS-based hybrid materials prepared by gamma irradiation." Radiation **Physics and Chemistry.** Vol.81 : 1336–1340.

[47] Jianliang Cao, Cong Qin, Yan Wang, Huoli Zhang, Guang Sun, and Zhanying Zhang. (2017) . "Solid-State Method Synthesis of SnO_2-Decorated g-C_3N_4 Nanocomposites with Enhanced Gas-Sensing Property to Ethanol." **Materials (Basel).** Vol.10(6) : 1-14.

[48] B. Bourlinos, Vasilios Georgakilas, Radek Zboril, Dalibor Jancik., Michael A. Karakassides, Andreas Stassinopoulos, Demetrios Anglos, Emmanuel P. Giannelis. "Reaction of graphite fluoride with NaOH–KOH eutecticAthanasios" (2008). **Journal of Fluorine Chemistry.** Vol.129 : 720–724.

APPENDIX

APPENDIX A

The fabrication of PDMS sponge.

To calculate the weight ratio of the compositions that were prepared to fabricate the PDMS sponge, we used the formula of Density that is a measure of relative compactness, or how heavy an object is relative to its size.

$$\rho = \frac{m}{v}$$

ρ = density ($kg \cdot m^3$)

m = mass (kg)

v = volume (m^3)

For example: To calculate the mass of PDMS and sacrifice templates that were used to prepare the sponge PDMS with dimensions of 7.3 x 7.3 x 0.4 cm^3. (Density of PDMS is 0.965 $g.cm^{-3}$, salt is 2.16 $g.cm^{-3}$)

$$m_{PDMS} = \rho V = 0.965\ g \cdot cm^{-3} \times 21.316\ cm^3$$

$$= 20.676\ g.$$

$$m_{Salt} = \rho V = 2.16\ g \cdot cm^{-3} \times 21.316\ cm^3$$

$$= 46.0\ g.$$

The fabrication of composite PDMS sponge.

For example: to calculate the mass of dispersed phase that was used to prepare the composite PDMS sponge. (A composite contains 3% by mass of g-C_3N_4 as dispersed phase)

$$m_{g.C_3N_4} = \frac{3\ g.\ of\ g.\ C_3N_4}{100\ g.\ of\ PDMS} \times 20.676\ g.\ of\ PDMS = 0.6\ g.\ of\ g.\ C_3N_4$$

Table A4.1 Data summary of the characteristics Flat and Sponge PDMS according to different templates.

Template	Compliance (MPa)	Contact angle (^{0})	Electrical properties		Dielectric properties	
			Voltage (Volt)	Current (μA)	Relative permittivity (at 1 MHz)	Dielectric loss
Flat PDMS	27.48	110.0±1.6	2.40±0.13	0.28±0.02	3.64	0.0016
CWS	98.40	116.3±1.5	1.40±0.10	0.08±0.01	1.88	0.0004
CBS	139.59	110.2±2.4	1.37±0.10	0.06±0.04	2.18	0.0014
WS	165.56	120.5±3.5	1.60±0.09	0.10±0.03	2.28	0.0012
BS	153.22	110.4±5.8	1.51±0.10	0.10±0.01	2.25	0.0006
MSG	151.15	125.3±3.5	1.74±0.12	0.12±0.01	2.29	0.0046
Salt	185.04	128.4±2.6	1.91±0.09	0.14±0.01	2.31	0.0007

Table A4.2 Data summary of the characteristics composite/PDMS sponge according to different disperse phases.

Disperse phases	Concentration (%wt)	Elastic modulus (MPa)	Contact angle (°)	Electrical properties		Dielectric properties	
				Voltage (Volt)	Current (μA)	Relative permittivity (at 1 MHz)	Dielectric loss
Graphite fluoride	10	NA	141.9±2.6	1.45±0.05	0.12±0.01	2.21	0.001
	20	0.56	132.8±1.5	1.45±0.07	0.14±0.01	2.51	0.0013
	40	0.85	138.1±4.9	1.82±0.11	0.20±0.01	3.55	0.0016
	60	0.86	141.0±5.2	1.51±0.07	0.16±0.01	2.49	0.0015
g-C_3N_4	1	0.49	NA	1.90±0.11	0.17±0.01	2.12	0.0004
	3	NA	143.1±2.1	1.69±0.12	0.11±0.01	2.13	0.0002
	5	0.51	142.0±2.3	2.12±0.19	0.13±0.01	2.32	0.0005
	10	0.68	143.6±2.9	1.71±0.15	0.09±0.01	2.49	0.0011

NA = no answer

Table A4.3 The value of the pore characterization by Measuring porosity and SEM.

Templates	Porosity (%)	Particle size of template by Optical camera (mm.)		Particle size of template by SEM (mm.)	Pore size by SEM (mm.)
-	0				
CBS	68				
CWS	72				
BS	57	wide	0.9625±0.173	0.4329±0.1621	0.4356±0.1476
		length	1.1508±0.209	0.5516±0.1397	0.7218±0.2506
WS	59	wide	0.7823±0.163	0.4853±0.1027	0.2817±0.1286
		length	0.9701±0.159	0.7528±0.1828	0.4470±0.2074
MSG	53	wide	0.5337±0.167	0.2531±0.0730	0.3635±0.1255
		length	2.2302±0.654	0.8994±0.4549	1.0072±0.2361
Salt	59	wide	0.6991±0.092	0.3654±0.0919	0.3889±0.0835
		length		0.3654±0.0919	0.3889±0.0835

To determine the Dielectric constant of the PDMS and composite PDMS sponge.

$$\text{Capacitance}(C) = \varepsilon_0 \varepsilon_r \cdot \frac{A}{d}$$

ε_0 = The vacuum permittivity (8.25×10^{-12} F.m^{-1})

ε_r = Relative permittivity or Dielectric constant (D)

A = Area

d = Thickness

Table A4.4 Data of the measured Capacitance of the flat and sponge PDMS.

Samples	Frequency (Hz)	Capacitance	Dielectric loss	d (m.)	A (m^2)
PDMS flat	10k	2.415179	0.001871	$5x10^{-3}$	$4x10^{-4}$
	100k	2.408885	0.00169	$5x10^{-3}$	$4x10^{-4}$
	1M	2.402086	0.001556	$5x10^{-3}$	$4x10^{-4}$
WS-PDMS sponge	10k	1.510712	0.003322	$5x10^{-3}$	$4x10^{-4}$
	100k	1.505877	0.001596	$5x10^{-3}$	$4x10^{-4}$
	1M	1.502026	0.001162	$5x10^{-3}$	$4x10^{-4}$
BS-PDMS sponge	10k	1.494953	0.002152	$5x10^{-3}$	$4x10^{-4}$
	100k	1.485925	0.001307	$5x10^{-3}$	$4x10^{-4}$
	1M	1.482433	0.000645	$5x10^{-3}$	$4x10^{-4}$
CWS-PDMS sponge	10k	1.261892	0.001373	$5x10^{-3}$	$4x10^{-4}$
	100k	1.244397	0.000776	$5x10^{-3}$	$4x10^{-4}$
	1M	1.239956	0.000412	$5x10^{-3}$	$4x10^{-4}$
CBS-PDMS sponge	10k	1.446219	0.003843	$5x10^{-3}$	$4x10^{-4}$
	100k	1.443212	0.001876	$5x10^{-3}$	$4x10^{-4}$
	1M	1.439686	0.001359	$5x10^{-3}$	$4x10^{-4}$
MSG-PDMS sponge	10k	1.528203	0.00206	$5x10^{-3}$	$4x10^{-4}$
	100k	1.522054	0.002979	$5x10^{-3}$	$4x10^{-4}$
	1M	1.513721	0.004643	$5x10^{-3}$	$4x10^{-4}$
Salt	10k	1.532899	0.005379	$5x10^{-3}$	$4x10^{-4}$
	100k	1.528369	0.00067	$5x10^{-3}$	$4x10^{-4}$
	1M	1.525118	0.000715	$5x10^{-3}$	$4x10^{-4}$

For example: To calculate the Dielectric constant of the PDMS flat in a frequency at 1 MHz.

$$\varepsilon_r = \frac{C \cdot d}{\varepsilon_0 A} = \frac{2.402086 \text{ x } 5.0\text{x}10^{-3}\text{m.}}{8.25\text{x}10^{-12}\ \text{F} \cdot \text{m}^{-1}\text{x } 4.0\text{x}10^{-3}\text{m}^2.} = 3.6\ \text{F} \cdot \text{m}^{-1}$$

To determine the %porosity of PDMS sponge.

Porosity can be measured of refractory materials using the Archimedes buoyancy technique with dry weights, soaked weights and immersed weights in solution.

Table A4.5 Data of the measured porosity by Archimedes buoyancy technique.

	Templates						
	-	CBS	CWS	BS	WS	MSG	Salt
Dry weight (w_1)	0.3822	0.8161	0.6250	0.9460	0.8214	0.8902	0.7710
Suspended weight (w_2)	0.0793	0.0873	0.0896	0.1301	0.0900	0.0807	0.1280
Soaked (w_3)	0.3830	2.1538	2.0915	1.9802	1.7982	1.7254	1.6601

The equation that was used to determine the %porosity.

$$\text{Total volume} = \frac{w_1 - w_2}{\rho_0}$$

$$\text{Open pore volume} = \frac{w_3 - w_1}{\rho_0}$$

$$\%\text{Porosity} = \frac{\text{Open pore volume}}{\text{Total volume}} \times 100$$

w_1 = dry weight

w_2 = Suspended Weight

w_3 = Soaked Weight

ρ_0 = density of ethanol

For example: To calculate %porosity of the PDMS sponge that was fabricated using salt as a sacrifice template. (Density of ethanol (at 34 °C) is 0.7751 g.cm^{-3})

$$\text{Total volume} = \frac{0.7710\ \text{g.} - 0.1280\ \text{g.}}{0.7751\ \text{g.cm}^{-3}} = 0.8296\ \text{cm}^3$$

$$\text{Open pore volume} = \frac{1.6601\ \text{g.} - 0.7710\ \text{g.}}{0.7751\ \text{g.cm}^{-3}} = 1.1471\text{cm}^3$$

$$\%\text{Porosity} = \frac{1.1471\text{cm}^3}{0.8296\ \text{cm}^3} \times 100 = 58$$

APPENDIX B

The electricity generation process of TENG

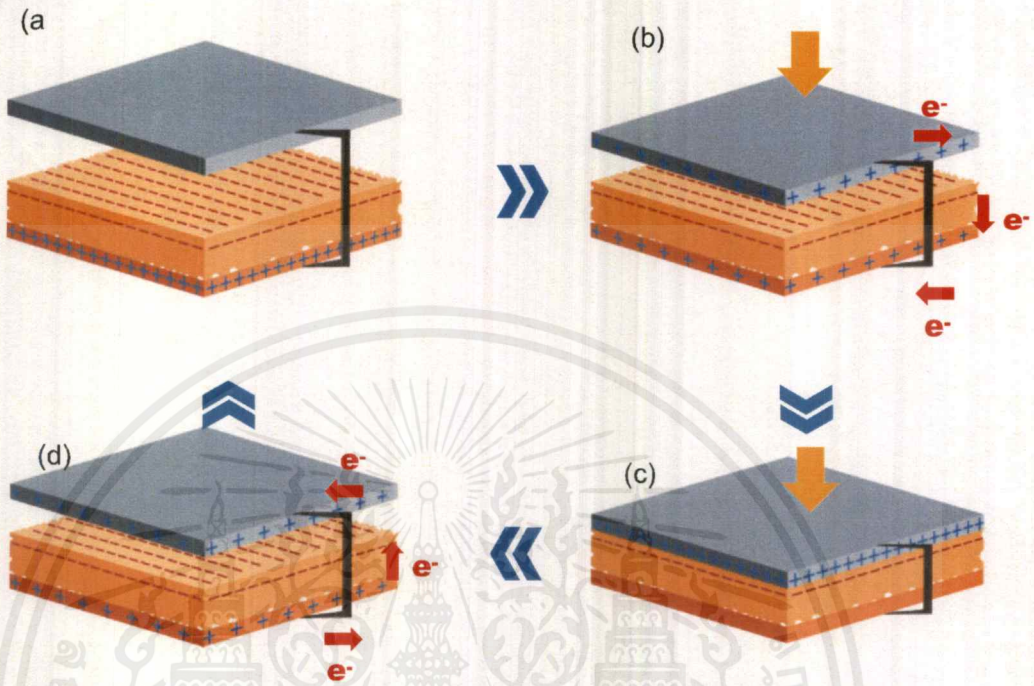

Figure S4.1 Schematic diagram of the electricity generation of the TENG.

(a) Original position without mechanical force applied. The electrons from back electrodes are injected into PDMS, resulting in surface triboelectric charges. At this stage, the TENG remains in electrostatic equilibrium state.

(b) When an external force is applied to the TENG, the electrostatic equilibrium is broken, electrons transfer from the top electrode to the back electrode, generating the positive current signal

(c) When an external force is applied to the TENG, the top electrode and PDMS are brought into contact, fiction occurs generating positive and negative triboelectric charges on the Al and PDMS surfaces.

(d) When the external force is released, the negative charges on the PDMS surface induce positive charges on the back electrode, thus, electrons on the back electrode move to the contact electrode through the external circuit, generating the negative current signal.

In the end, when the TENG reverts to the original position, all positive triboelectric charges on the contact electrode are neutralize.